Journal of Environmental Chemical Engineering 9 (2021) 105554

Contents lists available at ScienceDirect

Journal of Environmental Chemical Engineering

journal homepage: www.elsevier.com/locate/jece

Incorporation of ozone-driven processes in a treatment line for a leachate from a hazardous industrial waste landfill: Impact on the bio-refractory character and dissolved organic matter distribution

Inalmar D. Barbosa Segundo [a,b], Ana I. Gomes [a], Bianca M. Souza-Chaves [b,c], Minkyu Park [c], André B. dos Santos [d], Rui A.R. Boaventura [a], Francisca C. Moreira [a], Tânia F.C.V. Silva [a,*], Vítor J.P. Vilar [a,*]

[a] Laboratory of Separation and Reaction Engineering - Laboratory of Catalysis and Materials (LSRE-LCM), Departamento de Engenharia Química, Faculdade de Engenharia, Universidade do Porto, Rua Dr. Roberto Frias, 4200-465 Porto, Portugal
[b] CNPq - National Council for Scientific and Technological Development, Brazil
[c] Department of Chemical & Environmental Engineering, University of Arizona, 1133 E James E Rogers Way, Harshbarger 108, Tucson, AZ 85721-0011, USA
[d] Department of Hydraulic and Environmental Engineering, Federal University of Ceará, Campus do Pici, Bloco 713, Pici, CEP 60455-900 Fortaleza, Ceará, Brazil

ARTICLE INFO

Editor: Dr. GL Dotto

Keywords:
Industrial landfill leachate
Ozone-based AOPs
Biodegradability
Fluorescence excitation-emission matrix (3D-EEM)
Size-exclusion chromatography – organic carbon detection (SEC-OCD)

ABSTRACT

The current work aimed to evaluate the feasibility of including ozone (O_3)-based advanced oxidation processes (AOPs), as an intermediate step, in a multistage treatment system for non-biodegradable sulphur-rich leachate from a hazardous industrial solid waste landfill (HISWL), combining chemical and biological oxidation technologies. O_3-based AOPs covered perozonation (O_3/H_2O_2), photo-assisted ozonation (O_3/UVC), and photo-assisted perozonation (O_3/H_2O_2/UVC). All O_3-driven processes were applied to HISWL leachate directly after sulphur compounds removal via catalytic oxidation and chemical precipitation. Moreover, ozonation was also tested after a sequential coagulation step using ferric or aluminium salts (O_3/Fe^{2+} or O_3/Al^{3+}), and O_3/H_2O_2/UVC system was likewise tried after Fe-mediated coagulation targeting photo-Fenton-assisted ozonation (O_3/PF). The best-performing treatment train encompassed: (i) catalytic oxidation with H_2O_2 (stoichiometric amount) under free pH, to convert sulphite and sulphide ions into oxidised sulphur species, including sulphate; (ii) chemical precipitation of sulphate as barite mineral without pH correction; (iii) O_3/H_2O_2 process for ca. 2.1-h (natural pH; room temperature; 3.5 kg O_3 and 1.1 kg H_2O_2 per m^3 leachate), to degrade refractory organic matter and improve biodegradability; and (iv) biological oxidation to remove the remaining bioavailable organics fraction. This four-stage approach allowed shifting from a highly recalcitrant wastewater to an effluent in full agreement with the regulation for industrial wastewater discharge into the municipal sewer network. Furthermore, the effectiveness of the O_3/H_2O_2 process over the dissolved organic matter transformation was corroborated by fluorescence excitation-emission matrix and size exclusion chromatography analysis.

1. Introduction

Over the last few years, considerable progress has been made towards more recycling and alternative solid waste management techniques. Nonetheless, landfilling still continues to be in request, especially for hazardous waste disposal, as the most cost-effective method. As a result, the generation of leachates will be unavoidable, mainly due to rainwater percolation through the landfill and the decomposition of waste itself. Leachates from hazardous industrial solid waste landfills (HISWL) are a high-strength mixture that can contain dissolved hazardous organic compounds (including toxic and recalcitrant matter), inorganic constituents (e.g., ammonia, chloride and sulphide), heavy metals (e.g., arsenic, nickel and zinc) and xenobiotic organic compounds (such as halogenated organics). Their composition can broadly diverge regarding the stored waste type and compacting degree, local climatic conditions, geology and landfill age [1,2]. Proper landfill site management is of utmost importance to avoid the adverse environmental and health impacts associated with the

* Corresponding authors.
E-mail addresses: tania.silva@fe.up.pt (T.F.C.V. Silva), vilar@fe.up.pt (V.J.P. Vilar).

https://doi.org/10.1016/j.jece.2021.105554
Received 10 March 2021; Received in revised form 16 April 2021; Accepted 19 April 2021
Available online 27 April 2021

mistreated/untreated leachate release/spill, including, among others, surface waters and water/groundwater contamination, air pollution, and ecological habitats physical degradation. Given HISWL leachate complex and variable characteristics, there is no universal and cost-effective treatment solution able to ensure water resources protection. Notwithstanding, HISWL leachate treatment involves integrating different technologies, ranging from the conventional biological and physicochemical processes to the advanced oxidation processes (AOPs).

Several studies have been published concerning the applications of multistage treatment strategies for leachates from municipal solid waste landfills (MSWLs) [3–9]. However, information regarding the multi-step remediation of leachate from landfills receiving hazardous waste from multiple industries still lacks. To the best of our knowledge, besides two publications of our authorship [10,11], only four works were reported contemplating treatment trains for industrial leachates from non-hazardous waste landfills [2,12–14], and only one from a HISWL of a specific industry [15]. Previous studies conducted with this high-complexity HISWL leachate have revealed the need for a six-stage treatment system to meet the regulatory requirements composed of the following processes [10,11]: (i) catalytic oxidation (CO); (ii) chemical precipitation (CP); (iii) aerobic/anoxic biological oxidation; (iv) coagulation; (v) photo-Fenton (PF) reaction mediated by UVA radiation (PF-UVA); and (vi) aerobic biological oxidation. Despite the promising results, it was found that impractically long PF-UVA treatment times (i.e., >24 h) would be required to comply with the legal requirements for discharge of wastewater to aquatic systems such as a river. On the other hand, 4 h of operation was enough to achieve a water quality for discharge to a municipal sewer system. Moreover, even though their superior efficiency, the application of electrochemical processes, such as anodic oxidation or photoelectro-Fenton oxidation, replacing the PF-UVA reaction, has demonstrated to be unfeasible, mostly due to operational constraints related to the release of chlorine gas into the environment and generation of high amounts of foam, or the pore-clogging at the cathode surface [10].

Ozone (O_3)-based processes have become increasingly attractive with regard to the pre- or post-treatment of MSWL leachates [9,16–18], owing to the: (i) high oxidative power of the molecular O_3; (ii) high effectiveness in colour removal; (iii) high reactivity and selectivity towards organic compounds containing electron-rich moieties; (iv) generation of highly-reactive and non-selective hydroxyl radicals ($HO^{\bullet}$) under alkaline conditions (in contrast to the PF reaction); and (v) possible combination with hydrogen peroxide (H_2O_2) and/or UVC radiation, which also induces the production of $HO^{\bullet}$.

Accordingly, this study mainly focuses on the integration of ozonation and O_3-based AOPs (O_3/H_2O_2, O_3/UVC, and O_3/H_2O_2/UVC) in the multistage system aforementioned for the treatment of a particular HISWL leachate. Firstly, the main physicochemical parameters of the HISWL were determined (such as chemical and biochemical oxygen demand, dissolved organic carbon and nitrogen compounds content, and sulphur compounds concentration), in order to define the preliminary sequence of the integrated treatment strategy. The influence of inlet O_3 dosage on the mineralisation and oxidants consumption in ozonation and O_3/H_2O_2 processes was further assessed, using HISWL leachate after sulphur compounds removal. Then, under the best inlet O_3 dosage, the addition of UVC radiation to ozonation and O_3/H_2O_2 systems was also evaluated. Afterwards, the impact of an upstream coagulation process (using ferric or aluminium salts) on the ozonation (O_3/Fe^{2+} or O_3/Al^{3+}) and O_3/H_2O_2/UVC (O_3/PF) systems was also addressed. Moreover, the biodegradability enhancement along the best-performing process under the optimal conditions was determined by means of a Zahn-Wellens test. Finally, the heterogeneous character of the dissolved organic matter (DOM) of the HISWL leachate along the different treatment steps was also explored by fluorescence excitation-emission matrix (3D-EEM) and size-exclusion chromatography coupled with organic carbon detection (SEC-OCD).

2. Material and methods

2.1. Chemicals

Hydrogen peroxide (H_2O_2) 30% (w/v) and barium chloride dihydrate ($BaCl_2.2H_2O$) with purity > 99%, used as oxidising and precipitating agents in the catalytic oxidation and chemical precipitation processes, respectively, were both supplied by PanReac·H_2O_2 was also employed in some O_3-based AOPs. Ferric chloride ($FeCl_3$) 40% (w/w) and aluminium sulphate ($Al_2(SO_4)_3$) 48% (w/w) solutions, applied as coagulants, were purchase from Quimitécnica.com – Comércio e Indústria Química, S.A. and Rivaz Química, S.A., respectively. O_3 gas stream was generated from dry and high-purity (> 99.9%) oxygen (O_2), supplied by Linde, using an O_3 generator (BMT 802 N), able to produce up to 4 g O_3 h^{-1}. Concentrated hydrochloric acid (HCl) 33% (w/w) and sodium hydroxide (NaOH) with purity > 99%, employed for pH adjustment, were acquired from PanReac and Merck, respectively. Except for the commercial-grade coagulants, all the chemicals were of analytical grade. Demineralised and ultrapure water, used for analytical determinations, were obtained from a reverse osmosis system (Panice) and a Millipore® Direct-Q system (18.2 MΩ cm resistivity at 25 °C), respectively.

2.2. Raw leachate from a HISWL

Raw leachate was collected in May 2018 from a facultative pond (2800 m^3) installed at the leachate treatment plant (LTP) of a HISWL, located in the central region of Portugal, and stored at 4 °C until use. In operation since June 2008, the HISWL has mostly been receiving sludge from municipal wastewater treatment plants (MWWTPs) and soils containing heavy hydrocarbons, as well as waste from steelworks and mining and metallurgical industries. After the stabilisation pond, the LTP also includes an evaporation system where the leachate was pretreated. However, at that time, the poor quality of the effluent did not meet the limits for wastewater discharge to the sewer network of the local MWWTP. The main physicochemical characteristics of the raw leachate used in this work are shown in Table 1.

2.3. Analytical determinations

All the analytical methods applied along the experimental activities reported in the current work are described in the supplementary material (Table SM-1).

2.4. Experimental systems and procedures

2.4.1. Catalytic oxidation (CO) and chemical precipitation (CP)

CO and CP processes were employed to remove sulphur compounds from the raw leachate under the best-operating conditions found in a previous study [11], regarding the pre-treatment of a leachate collected two years early from the same HISWL as the one reported in the current paper.

In a first stage, about 80 L of raw leachate were introduced into a 100 L batch stirred tank reactor, where the sulphide and sulphite ions were catalytically oxidised by the addition of H_2O_2 as oxidant agent (5-min total stirring time - to homogenisation and oxidation reaction, natural pH and room temperature), getting $[H_2O_2]$:$[S^{2-}]$ and $[H_2O_2]$:$[SO_3^{2-}]$ molar proportions of 4:1 and 1:1, respectively. Transition metals available in leachate acted as catalysts, as concluded in Barbosa Segundo et al. [11]. After settling the chemical sludge overnight (about 16 h), leachate containing oxidised sulphur species, including sulphate, was then withdrawn from the reactor.

In a second stage, the clarified pre-oxidised HISWL leachate (about 77 L) was placed into another 100 L batch stirred tank reactor, where the sulphate ions were chemically precipitated as barite (30-min stirring time, natural pH and room temperature) by the addition of $BaCl_2.2H_2O$,

Table 1
Physicochemical characteristics of the HISWL leachate throughout the various stages of the best treatment strategy.

Parameter (unit)	Raw leachate	After CO[a]	After CP[b]	After O_3/H_2O_2[c]	After BO[d]	EVL[e]	MCV[f]
Colour	Light brown	Light brown	Light yellow	n.d.	n.d.		
Colour (diluted 1:20)	d.	d.	d.	n.d.	n.d.	n.d. (dil. 1:20) or n.c.	n.c.
Colour (Pt-Co units)	760	760	500	<15[g]	<15[g]		
Odour	Very strong	Strong	Low	n.d.	n.d.		
Odour (diluted 1:20)	d.	d.	d.	n.d.	n.d.	n.d. (dil. 1:20) or n.c.	n.c.
pH	8.4	8.6	8.9	8.1	7.0	6.0–9.0 or n.c.	5.5–9.5
Alkalinity (mg $CaCO_3$ L^{-1})	2427	2139	1921	1664	1016		
Turbidity (NTU)	29	22	19	1.2	1.5		
Total suspended solids – TSS (mg L^{-1})	157	n.m.	131	n.m.	31	60 or 35	1000
Total volatile solids – VSS (mg L^{-1})	87	n.m.	68	n.m.	13		
Total dissolved carbon – TDC (mg L^{-1})	1548	1214	1085	768	508		
Dissolved inorganic carbon – DIC (mg L^{-1})	582	508	448	405	304		
Dissolved organic carbon – DOC (mg L^{-1})	966	706	637	363	276		
Chemical oxygen demand – COD (mg O_2 L^{-1})	2809	2127	1970	980	708	150 or 125	1000
COD/DOC	2.9	3.0	3.1	2.7	2.6		
5-day biochemical oxygen demand – BOD_5 (mg O_2 L^{-1})	360	250	250	n.m.	n.m.	40 or 25	500
BOD_5/COD	0.13	0.12	0.13	n.m.	n.m.		
Biodegradability - Zahn-Wellens test (%)	12	n.m.	11	24	n.m.		
Absorbance at 254 nm (AU) (diluted 1:50)	0.75	0.72	0.54	0.011	0.013		
Transmittance at 254 nm (%) (diluted 1:50)	18	19	29	97	97		
$SUVA_{254}$ (L mg^{-1} m^{-1})	3.88	5.12	4.26	0.15	0.24		
Total nitrogen – N_T (mg L^{-1})	260	n.m.	165	105	80	15 or 10	90
Ammonium – N-NH_4^+ (mg L^{-1})	220	n.m.	140	75	50	7.8 or n.c.	77
Nitrate – N-NO_3^- (mg L^{-1})	20	n.m.	13	15	10	11 or n.c.	11
Nitrite – N-NO_2^- (mg L^{-1})	<0.05[g]	n.m.	<0.05[g]	<0.05[g]	<0.05[g]		
Sulphate – SO_4^{2-} (mg L^{-1})	4943	6404	548	558	565	2000 or n.c.	1000
Sulphite – SO_3^{2-} (mg L^{-1})	2575	<1.0[g]	<1.0[g]	<1.0[g]	<1.0[g]	1.0 or n.c.	n.c.
Sulphide – S^{2-} (mg L^{-1})	450	<0.1[g]	<0.1[g]	<0.1[g]	<0.1[g]	1.0 or n.c.	1.0
Chloride – Cl^- (g L^{-1})	14.5	13.8	19.7	19.3	19.0		
Total phosphorous – P_T (mg L^{-1})	2.25	n.m.	n.m.	n.m.	0.85	10 or 1.0	20
Total aluminium – Al (mg L^{-1})	<5.0[g]	n.m.	n.m.	n.m.	n.m.	10 or n.c.	10
Total barium – Ba (mg L^{-1})	<0.61[g]	n.m.	n.m.	n.m.	n.m.		
Total cadmium – Cd (mg L^{-1})	<0.05[g]	n.m.	n.m.	n.m.	n.m.	0.2 or n.c.	n.c.
Total copper – Cu (mg L^{-1})	0.14	n.m.	n.m.	n.m.	n.m.	1.0 or n.c.	1.0
Total iron – Fe (mg L^{-1})	1.26	n.m.	n.m.	n.m.	n.m.	2.0 or n.c.	2.5
Total lead – Pb (mg L^{-1})	<0.21[g]	n.m.	n.m.	n.m.	n.m.	1.0 or n.c.	1.0
Total manganese – Mn (mg L^{-1})	0.17	n.m.	n.m.	n.m.	n.m.		
Total nickel – Ni (mg L^{-1})	<0.15[g]	n.m.	n.m.	n.m.	n.m.		
Total zinc – Zn (mg L^{-1})	0.23	n.m.	n.m.	n.m.	n.m.	2.0 or n.c.	5.0

d. – detected; n.d. – not detected; n.c. – not covered; n.m. – not measured; dil. – diluted.

[a] Using the raw HISWL leachate. Catalytic oxidation (CO) conditions: room temperature; natural pH; stirring time of 5 min; $[H_2O_2]$:$[S^{2-}]$ molar ratio = 4:1; $[H_2O_2]$:$[SO_3^{2-}]$ molar ratio = 1:1, subsequent sedimentation overnight and removal chemical sludge.

[b] Using the HISWL leachate after CO. Chemical precipitation (CP) conditions: room temperature; natural pH; stirring time of 30 min; $[Ba^{2+}]$:$[SO4^{2-}]$ molar ratio of 1:1; subsequent sedimentation overnight and removal barite precipitate.

[c] Using the HISWL leachate after sequential CO and CP. Perozonation process (O_3/H_2O_2) conditions: room temperature; natural pH; OD_{inlet} of 40 mg O_3 L^{-1}; $[H_2O_2]$ = 200–500 mg L^{-1}; contacting time of 3 h; subsequent sedimentation for 3 h and removal of O_3/H_2O_2 sludge (when required).

[d] Using the HISWL leachate after sequential CO, CP and O_3/H_2O_2 process. Biological oxidation (BO) conditions: 28 days Zahn-Wellens test, subsequent sedimentation for 2 h and removal of the biological treatment sludge.

[e] ELV - Emission limit value for discharge into water bodies according to Decree-Law 236/98 (Portuguese legislation) or Directive 91/271/CEE (European legislation).

[f] MCV - Maximum concentration values for the rejection of industrial wastewater into the municipal sewage system of the Vila Nova de Gaia municipality (Regulation no. 143/2018 published in Diário da República no. 46/2018, series II of 2018–03–06).

[g] Limit of detection.

using a $[Ba^{2+}]$:$[SO_4^{2-}]$ molar ratio of 1:1. Finally, about 75 L of the desulphurised HISWL leachate was withdrawn from the reactor after the sedimentation of the barite mineral overnight (about 16 h) and stored at 4 °C until its use in the subsequent trials.

2.4.2. Coagulation

In order to assess the influence of the pre-treatment type on a downstream O_3-based process, coagulation of the near-sulphur-free leachate was performed using: (i) a ferric salt ($FeCl_3$) at acidic medium, under the best conditions (100 mg Fe^{3+} L^{-1}; pH 2.8) reported in a former work [10], using a leachate from the same HISWL; and (ii) an aluminium salt ($Al_2(SO_4)_3$) at free near-neutral pH conditions, whose dose was optimised in a *jar-test* apparatus (Velp Scientifica, model JLT6). The addition of flocculants (anionic polyacrylamide Magnafloc 155 or cationic polyacrylamide Ambifloc C 58) to the coagulated leachate showed no improvements (data not shown since there was no change on DOC or turbidity values after flocculants addition).

Regarding jar-tests, the general procedure was as follows: (i) introduction of 250 mL of desulphurised HISWL leachate into 500 mL beakers; (ii) pH adjustment (when required); (iii) addition of $Al_2(SO_4)_3$; (iv) pH correction (when required); (v) rapid mixing (120 rpm) during 3 min; (vi) slow mixing (20 rpm) during 20 min; (vii) 2 h settling; and (viii) withdraw of the clarified leachate for dissolved organic carbon (DOC) and turbidity measurement. Following this general procedure, the optimisation of the coagulation process was divided into two parts. Firstly, in the presence of 300 mg Al^{3+} L^{-1} of coagulant, the effect of pH was evaluated according to three approaches: (i) coagulation at natural pH, without a further correction after the coagulant addition; (ii) coagulation at natural pH, with a further correction to its initial value after the coagulant addition; and (iii) coagulation with initial pH adjustment to 6 and further correction to its initial value after the coagulant addition. Secondly, for the best pH condition, the influence of

the $Al_2(SO_4)_3$ dose was assessed between 100 and 400 mg Al^{3+} L^{-1}.

In order to obtain coagulated HISWL leachate in quantity enough to the subsequent trials, a cylindrical reaction vessel was filled with 5 L of desulphurised HISWL leachate, the pH was adjusted to the best value (when required), the optimal $FeCl_3/Al_2(SO_4)_3$ dose was added and the mechanical stirring was triggered for 3 min at 120 rpm followed by 20 min at 20 rpm. Lastly, clarified coagulated HISWL leachate was carefully withdrawn after a 2 h sedimentation period.

2.4.3. O_3-driven processes

All the experiments for ozonation and O_3-based AOPs (O_3/H_2O_2, O_3/UVC, and $O_3/UVC/H_2O_2$) were performed in a semi-batch lab-scale unit (see Fig. 1) mainly composed of: (i) a recirculation glass column (BMT, model 4.1), with a 73 mm internal diameter and a 370 mm maximum fluid height; (ii) a 680 mL capacity annular channel photoreactor, designated by FluHelik, coupled in series with the column; (iii) a gear pump (Ismatec, model BVP-Z), to promote the leachate recirculation between the column and the FluHelik (flow rate of 75 L h^{-1}); and (iv) a Venturi injector placed at the photoreactor inlet, to inject a continuous flow of an O_3/O_2 gaseous mixture into the recirculating liquid stream. More detailed information about this system setup can be consulted in Gomes et al. [9]. The FluHelik photoreactor is fully described elsewhere [19] and mainly comprised of: (i) an outer cylindrical shell made of borosilicate glass, with inlet and outlet pipes positioned perpendicularly to the fluid flow direction and tangentially to the shell, in horizontal plane and at the top in opposite sides; and (ii) a concentric inner quartz tube filled with a UVC low-pressure mercury lamp (Philips TUV 11 W G6T5, with useful power of 2.5 J s^{-1} determined by H_2O_2 actinometry). Inlet and outlet O_3 concentrations in the gas phase were monitored by a UV-based O_3 analyser (BMT, model 964), after dehumidification (BMT dehumidifier, model DH3b). Unreacted O_3 gas leaving the system was directed to a catalytic O_3 destruction unit (Heated Catalytic BMT) and further bubbled into Woulff bottles filled with 2% KI solution. All system units were connected by PTFE tubing.

Firstly, inlet O_3 concentration ($[O_3]_{in}$) and gas flow rate (Q_{gas}) were set for 134, 200, or 167 mg O_3 L^{-1} and 0.15, 0.24, or 0.30 L min^{-1} to achieve inlet O_3 doses (OD_{inlet}) of 20, 30, 40 and 50 mg O_3 min^{-1}. During ca. 20–30 min, the O_3 gas stream was diverted to the O_3 analyser until the complete stabilisation of the O_3 generation process. Meanwhile, 1.5 L of HISWL leachate was fed to the glass column and recirculated for 10–20 min in the dark. Three HISWL leachate samples were used in the trials: (i) HISWL leachate after CO and CP, or desulphurised HISWL leachate; (ii) HISWL leachate after CO, CP and coagulation with iron salt, hereinafter referred to as Fe-coagulated HISWL leachate; and (iii) HISWL leachate after CO, CP and coagulation with aluminium salt, hereinafter referred to as Al-coagulated HISWL leachate. After the stabilisation period and before directing the O_3/O_2 gas stream to the Venturi injector, the first control sample was taken at a sampling point located between the FluHelik and the column. Experiments started with the injection of O_3 gas into the liquid stream through the Venturi injector and, for the O_3-based AOPs, also by: (i) the addition of 500 mg L^{-1} of H_2O_2 for O_3/H_2O_2 process; (ii) turning on the UVC lamp for O_3/UVC reaction; or (iii) the provision of 500 mg L^{-1} of H_2O_2 together with the UVC lamp switch on for $O_3/UVC/H_2O_2$ system. In the trials where H_2O_2 was a requirement, it was periodically supplied to maintain its concentration in the range 200–500 mg L^{-1}, except for one test where it was added all at once for comparison purposes. All tests were carried out for 3 h in the absence of temperature and pH control. Leachate samples were regularly taken for process control, every 20 min during the first hour and every 30 min during the remaining ones.

A PF ($Fe^{2+}/H_2O_2/UVC$) reaction was also performed as a blank control experiment, at pH 2.8 with Fe-coagulated HISWL leachate.

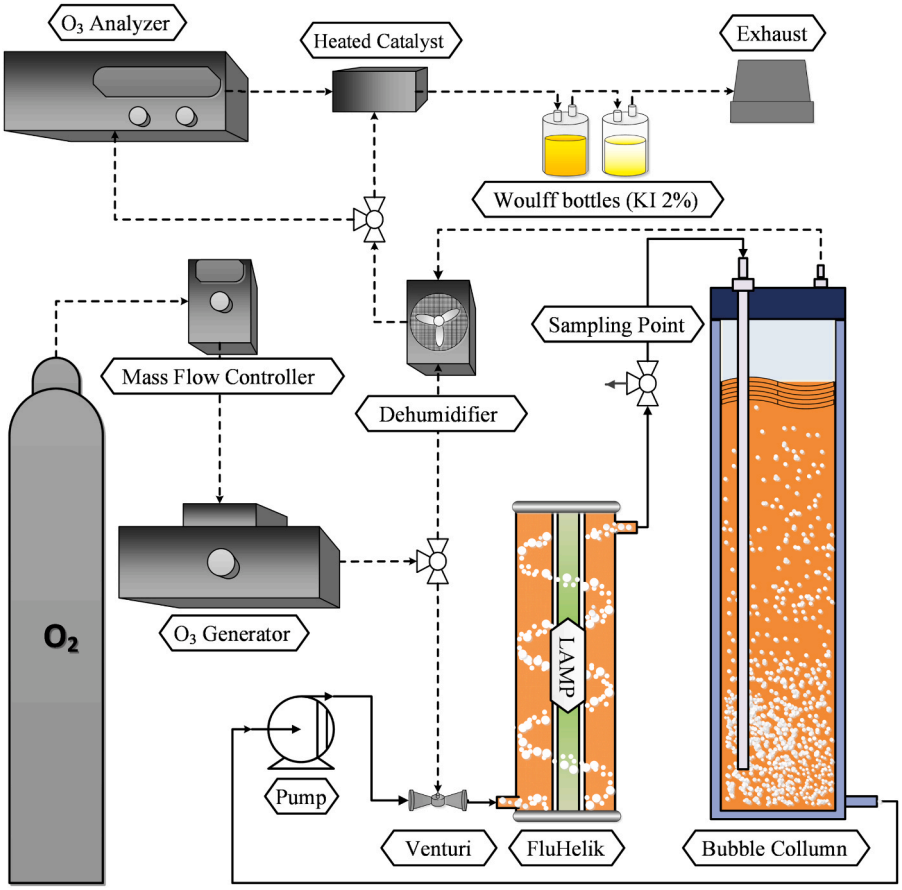

Fig. 1. Sketch of the O_3-driven processes lab-scale flow system.

Moreover, the PF reaction was considered the best process among the other ones applied in a previous study [10] using a leachate collected from the same HISWL. The experimental procedure was identical to the above-mentioned, but O_3 was not used.

The efficiency of the O_3-based processes was evaluated and compared in terms of DOC removal as a function of (i) reaction time by fitting a pseudo-first-order kinetic model to the experimental data; and (ii) O_3 and H_2O_2 consumption by fitting a pseudo-zero-order kinetic model to the experimental data. O_3 consumed at each treatment time was estimated as the transferred O_3 dose (TOD, g O_3 L^{-1} effluent), which depicts the accumulated amount of O_3 in the gas phase that is transferred to the liquid phase per unit of volume and time, according to Eq. (1).

$$TOD = \int_o^t \frac{Q_{gas}}{V_{liq}} \left([O_3]_{in} - [O_3]_{out} \right) dt \quad (1)$$

where t is the contact time (min), Q_{gas} is the gas flow rate (L min^{-1}), V_{liq} is the volume of the leachate in the reactional system (L), and $[O_3]_{in}$ and $[O_3]_{out}$ are the inlet and outlet concentrations of O_3 in the gas phase (g L^{-1}), respectively.

Additionally, a rough estimate of the operating costs associated with the best O_3-based treatment and respective operating conditions was also performed, taking into consideration the: (i) total O_3, O_2 (used to generate O_3) and H_2O_2 dose fed to the system during the necessary contacting time to achieve an intended mineralisation degree; (ii) energy consumed to generate the feeding O_2/O_3 gas stream (15 kWh kg^{-1} O_3 [20], when pure O_2 is fed to the O_3 generator); and (iii) unitary costs related to electric energy (0.10 € kWh^{-1}, the average market price for industrial applications), as well as pure O_2 and H_2O_2 solution at 50% (w/v) (0.14 € m^{-3}, and 375 € ton^{-1}, respectively, market prices of Portuguese companies).

3. Results and discussion

3.1. Considerations on the raw and desulphurised HISWL leachate

Table 1 displays the main physicochemical features of the raw HISWL leachate, as well as the HISWL leachate after undergoing all treatment steps in the best conditions. Overall, the leachate sample used in this study presents better characteristics than the one collected from the same HISWL to perform previous studies as reported elsewhere [10,11], highlighting the: (i) colour (63% clearer); (ii) alkalinity (57% inferior); (iii) organic matter content (DOC and COD was 58% and 60% lower, respectively); (iv) total nitrogen and ammonium nitrogen (52% and 33% minor, respectively); and (v) sulphates (61% lesser). Notwithstanding, taking into account the raw HISWL leachate characteristics and emission limit values (ELV), presented in Table 1, it can be concluded that the removal of sulphur, organic and nitrogen compounds is mandatory. Therefore, an effluent in compliance with the current legislation could only be achieved by combining conventional chemical (for sulphur compounds and/or colloidal particles removal) and biological (for nitrogen and biodegradable organic matter removal) processes with AOPs (for recalcitrant organics degradation), as already demonstrated for both industrial and urban landfill leachates [3,8–10,12].

Before HISWL leachate is subjected to a subsequent O_3-based or biological oxidation stage, the elimination of the high sulphur content is crucial to minimise O_3 consumption [21,22] or to decrease toxicity to microorganisms (especially nitrifiers) [23,24], respectively. Hence, HISWL leachate's desulphurisation was achieved by CO and CP, similar to what was performed in previous studies [10,11]. As could be seen from Table 1, in the current work: (i) CO converted more than 99.9% of sulphites and sulphides into oxidised sulphur species, with the partial formation of sulphate (c.a. 33%), using H_2O_2 stoichiometric amount (considering full oxidation into sulphates [25,26]) and leachate transition metals themselves as catalysts at natural pH; and (ii) CP removed more than 90% of sulphates under the form of barite mineral, with potential commercial value (after purification), for instance, as oil well drilling fluid constituent, adhesives/plastics/paints/rubber filler and polymers mechanical proprieties improver [11], using barium salt stoichiometric amount at natural pH. Furthermore, contrary to the previous studies with a leachate from the same landfill [10,11], in this case: (i) during the CO process, a milky-white precipitate was generated along with an alkalinity (12%) and DOC (27%) reduction (see Table 1), most likely due to the carbonate/calcium salts precipitation and organic matter coprecipitation or volatilisation (as larger leachate volumes have been handled); and (ii) after the CP process, bacteria activity did not increase, hindering the application of a downstream biological oxidation process.

At the end of the sequential CO and CP processes, the desulphurised HISWL leachate presented concentrations of sulphate, sulphite, and sulphide ions of 548, <1.0, and <0.1 mg L^{-1}, thus fulfilling the Portuguese legal discharge requirements (2000 mg L^{-1}, 1.0 mg L^{-1} and 1.0 mg L^{-1}, respectively), and low suitability for biodegradation (see Table 1). Accordingly, the next treatment step went through an O_3-based process, with the potential incorporation of a conventional coagulation process upstream.

3.2. Ozonation and O_3-driven processes

The kinetics of DOC abatement in all O_3-based reactions followed a pseudo-first-order kinetic model (determination coefficient (R^2) > 0.98 and residual variance (S^2_R) < 3.6×10^{-4} mg^2 L^{-2}). On the other side, the amount of DOC removed as a function of the oxidant consumed, either O_3 or H_2O_2, followed a linear correlation (R^2 > 0.99). All the correspondent kinetic constants are displayed in the Table 2.

3.2.1. Effect of the inlet O_3 dose

O_3 dose is a key operating parameter when economic viability is envisioned, mainly dealing with the treatment of high-polluted industrial wastewaters. To assess the effects of inlet O_3 dose (OD_{inlet}) on the reaction performance, the gas flow rate (Q_{gas}) and the inlet O_3 gas concentration ($[O_3]_{in}$) were manipulated. Interestingly, controlling OD_{inlet} by changing $[O_3]_{in}$ substantially influenced DOC degradation. As shown in Fig. 2a,b and Table 2, the increase in $[O_3]_{in}$ from 134 to 200 mg O_3 L^{-1} with a constant Q_{gas} (0.15 L min^{-1}) resulted in 1.5-fold higher DOC removal, suggesting that the extent of DOC degradation (more 10% after 3-h reaction) was linearly proportional to the available O_3 content. Moreover, in both reactions (i) very low O_3 concentrations were detected in the off-gas stream, being the O_3 utilisation ratios equal to 0.96 (Fig. 2a: inset), and (ii) a similar O_3 specific consumption was found (Fig. 2c), being the amount of DOC removed per gram of O_3 transferred between 55 ± 4 and 56 ± 4 mg C g^{-1} O_3. These results are consistent with the work carried out by Moslemi et al. [27], where it was reported that the dissolved O_3 concentration was proportional to the $[O_3]_{in}$ when the Q_{gas} was kept constant. The enhancement in the O_3 dissolution as a result of higher inlet O_3 concentrations was attributed to the O_3 deficit term of the mass transfer rate since the O_3 mass transfer coefficient was not considerably affected over the studied O_3 concentration range.

In contrast, controlling OD_{inlet} by Q_{gas} did not significantly affect the mineralisation of organic carbon. The increase in Q_{gas} from 0.24 to 0.30 L min^{-1} with a constant $[O_3]_{in}$ (167 mg O_3 L^{-1}) resulted in similar pseudo-first-order rate constants (i.e., 2.3 ± 0.2 and 2.1 ± 0.1 min^{-1}, respectively), which are not statistically different (with a confidence level of 95%) (Fig. 2a, b). In addition, the increase in Q_{gas} to increase OD_{inlet} considerably reduced the O_3 utilisation and O_3 consumption efficiency. For instance, as OD_{inlet} increased from 40 to 50 mg O_3 min^{-1} by elevating Q_{gas}, the O_3 utilisation ratio dropped from 0.88 to 0.81 (Fig. 2a: inset), while the O_3 consumption efficiency declined from 52 ± 3 to 40 ± 2 mg C g^{-1} O_3 (Fig. 2c). This behaviour may be closely

Table 2
Operating conditions and kinetic parameters in terms of DOC degradation for each O_3-driven reaction.

#	Experiment[a]	OD_{inlet} (mg O_3 min^{-1})	$[O_3]_{in}$ (mg O_3 L^{-1})	Q_{gas} (L min^{-1})	TOD[b] (g O_3 L^{-1})	H_2O_2[b] (g L^{-1})	$DOC_{rem.}$[b] (%)	Kinetics (time)			Kinetics (TOD)		Kinetics (H_2O_2)	
								k[c] ($\times 10^{-3}$ min^{-1})	R^2	S^2_R (mg^2 L^{-2})	k_{TOD}[d] (mg C g O_3^{-1})	R^2	k_{H2O2}[d] (mg C g $H_2O_2^{-1}$)	R^2
Effect of the inlet O_3 dose (Fig. 2)														
1.1	Ozonation_20 mg O_3 min^{-1}	20	134	0.15	2.42	–	19.7	1.3 ± 0.1	0.990	5.30×10^{-5}	55 ± 4	0.994	–	–
1.2	Ozonation _30 mg O_3 min^{-1}	30	200	0.15	3.61	–	29.6	2.0 ± 0.1	0.995	5.79×10^{-5}	56 ± 4	0.997	–	–
1.3	Ozonation _40 mg O_3 min^{-1}	40	167	0.24	4.38	–	34.5	2.3 ± 0.2	0.992	1.16×10^{-4}	52 ± 3	0.996	–	–
1.4	Ozonation _50 mg O_3 min^{-1}	50	167	0.30	5.06	–	31.7	2.1 ± 0.1	0.996	4.95×10^{-5}	40 ± 2	0.998	–	–
Effect of the H_2O_2 addition (Fig. 2)														
2.1	$O_3/H_2O_{2(SD)}$_30 mg O_3 min^{-1}	30	200	0.15	3.76	1.42	34.1	2.3 ± 0.2	0.991	1.39×10^{-4}	57 ± 3	0.996	127 ± 8	0.996
2.2	O_3/H_2O_2_30 mg O_3 min^{-1}	30	200	0.15	3.72	1.26	36.9	2.4 ± 0.2	0.987	2.27×10^{-4}	64 ± 4	0.997	182 ± 9	0.997
2.3	O_3/H_2O_2_40 mg O_3 min^{-1}	40	167	0.24	4.97	1.71	43.0	3.0 ± 0.1	0.997	6.22×10^{-5}	57 ± 3	0.995	(17 ± 2)× 10	0.989
2.4	O_3/H_2O_2_50 mg O_3 min^{-1}	50	167	0.30	6.24	1.82	45.2	3.1 ± 0.3	0.987	3.51×10^{-4}	47 ± 3	0.998	(17 ± 1)× 10	0.995
Effect of the UVC irradiation exposure (Fig. 3)														
1.2	Ozonation	30	200	0.15	3.61	–	29.6	2.0 ± 0.1	0.995	5.79×10^{-5}	56 ± 3	0.997	–	–
2.2	O_3/H_2O_2	30	200	0.15	3.72	1.26	36.9	2.4 ± 0.2	0.987	2.27×10^{-4}	64 ± 4	0.997	182 ± 9	0.997
3.1	O_3/UVC	30	200	0.15	3.58	–	30.7	2.0 ± 0.1	0.994	6.77×10^{-5}	56 ± 2	0.996	–	–
3.2	O_3/H_2O_2/UVC	30	200	0.15	3.71	1.62	37.9	2.5 ± 0.2	0.984	3.04×10^{-4}	66 ± 2	0.997	149 ± 8	0.997
3.3	H_2O_2/UVC	–			–	0.32	–	–	–	–	–	–	–	–
Effect of the HISWL leachate pre-treatment (Fig. 4)														
1.2	Ozonation	30	200	0.15	3.61	–	29.6	2.0 ± 0.1	0.995	5.79×10^{-5}	56 ± 3	0.997	–	–
3.2	O_3/H_2O_2/UVC	30	200	0.15	3.71	1.62	37.9	2.5 ± 0.2	0.984	3.04×10^{-4}	66 ± 2	0.997	149 ± 8	0.997
4.1	Al-Coag./ozonation	30	200	0.15	2.94	–	16.6	1.02 ± 0.06	0.991	3.07×10^{-5}	27 ± 3	0.997	–	–
4.2	Fe-Coag./ozonation	30	200	0.15	2.51	–	16.2	1.01 ± 0.04	0.996	1.26×10^{-5}	31 ± 3	0.996	–	–
4.3	Fe-Coag./O_3/H_2O_2/UVC	30	200	0.15	3.70	1.71	23.9	1.5 ± 0.1	0.993	5.55×10^{-5}	33 ± 2	0.998	74 ± 4	0.996
4.4	Fe-Coag./H_2O_2/UVC	–	–	–	–	1.01	14.1	0.61 ± 0.04	0.991	1.19×10^{-5}	–	–	50 ± 3	0.996

[a] All experiments were performed for 3 h, at room temperature and without pH correction. Initial pH was 8.9, except for trials #4.1 and #4.2-"4.4 that was 4.8 and 2.7, respectively. Initial DOC was 637 ± 24 mg L^{-1}, except for trials #4.1-#4.4 that was 499 ± 6 mg L^{-1}. In trials #3.1-#3.3 and #4.3-#4.4, an 11 W UVC lamp was used. During the trials #2.3-#2.4, #3.2-#3.3 and #4.3-#4.4, H_2O_2 several doses were periodically added to keep its concentration in the range 0.2–0.5 g L^{-1}. In trial #2.1, H_2O_2 was added as a single dose (SD) of 1.5 g L^{-1}.

[b] TOD, H_2O_2, and $DOC_{rem.}$ are the total (i) transferred O_3 dose, (ii) consumed H_2O_2 content, and (iii) removed DOC percentage, after 3-h reaction.

[c] Pseudo-first-order kinetic constant (k) for DOC degradation, determined though nonlinear regression method by minimising the sum of the squared deviations between the experimental and the predicted values. The goodness of fitting was evaluated by the coefficient of determination (R^2) and residual variance (S^2_R).

[d] DOC degradation reaction rates expressed in terms of O_3 transferred and H_2O_2 consumed.

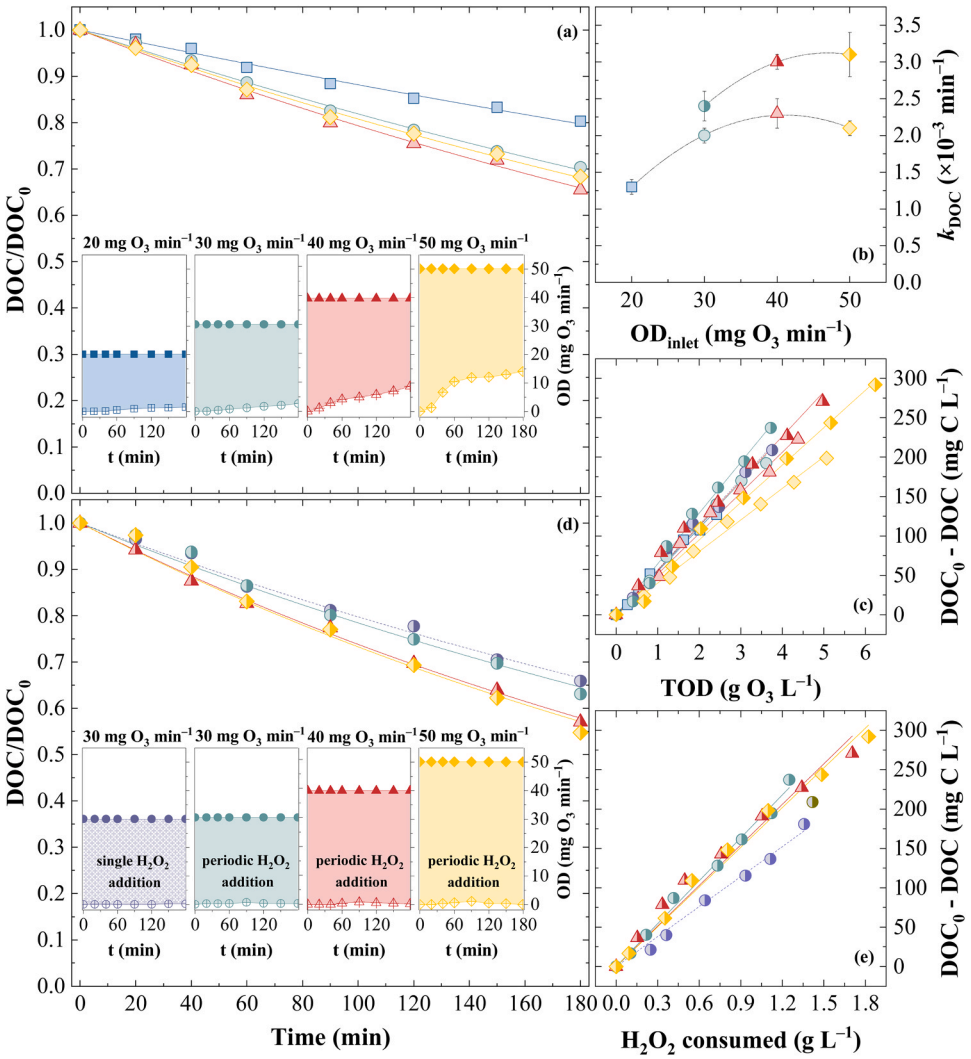

Fig. 2. Evolution of the: (a, d) normalised DOC reduction (symbols) over time, along with the respective pseudo-first-order fitting curves (lines); (b) kinetic constants for each inlet O_3 dose (OD_{inlet}) tested; and total DOC removed as a function of the (c) transferred O_3 dose (TOD) and (e) H_2O_2 consumed; during the ozonation process (a; filled symbols) and the O_3/H_2O_2 process (b; semi-filled symbols), using different OD_{inlet}: 20 (□), 30 (○,◑,◑), 40 (△,◭), and 50 (◇,◆) mg O_3 min^{-1}. Inset: Representation of the inlet (solid symbols) and outlet (crossed symbols) O_3 dose over time, where the shaded areas correspond to the total amount of O_3 available for the reaction. Experimental conditions: $[DOC]_0 = 637 \pm 24$ mg L^{-1}; $V = 1.5$ L; room temperature; $pH_0 = 8.9 \pm 0.2$; $[H_2O_2] =$ 200–500 mg L^{-1} (periodic addition) (solid line) or $[H_2O_2] = 1500$ mg L^{-1} (single addition) (dotted line and patterned area) – except when indicated.

related to O_3 mass transfer limitations [28]. Under a fixed contaminant load and inlet O_3 concentration, when the Q_{gas} is increased the O_3 dosage also increases in the same period of time, which boosts the ozonation process, until a certain point. Nevertheless, when the O_3 input rate exceeds the O_3 consumed by the ozonation reactions, the DOC removal efficiencies became independent of the Q_{gas}, since the rate-limiting-step, i.e. the O_3 mass transfer, is turned into a kinetically controlled regime [28]. Besides, as the Q_{gas} rises, O_3 losses also rise, suggesting that, for this reactional system, the use of lower inlet gas flow rates could be more suitable [27].

It is well established that O_3 reacts with organic and inorganic species in an aqueous solution with two kinetic regimes [29,30]: (i) direct reaction of molecular O_3 (redox potential (E^o) of 2.08 V/SHE), mainly under acidic conditions (pH < 4), with high selectivity for unsaturated electron-rich bonds of specific functional groups, such as aromatics, amines, and olefins, but fairly slow; and (ii) indirect reaction of secondary oxidisers generated by O_3 decomposition via Eqs. (2)–(14), such as the H_2O_2 and, most important, the powerful and non-selective hydroxyl radicals ($HO^\bullet$) (E^o of 2.73 V/SHE), which are rapidly and preferentially yielded at alkaline conditions (pH > 9).

$$O_3 + HO^- \rightarrow HO_2^- + O_2 \quad (2)$$

$$HO_2^- + O_3 \rightarrow O_3^{\bullet -} + HO_2^\bullet \quad (3)$$

$$HO_2^\bullet \rightarrow O_2^{\bullet -} + H^+ \quad (4)$$

$$O_2^{\bullet -} + H^+ \leftrightarrow HO_2^\bullet \quad (5)$$

$$O_2^{\bullet -} + O_3 \rightarrow O_3^{\bullet -} + O_2 \quad (6)$$

$$O_3^{\bullet -} + H_2O \rightarrow HO^\bullet + O_2 + HO^- \quad (7)$$

$$O_3^{\bullet -} + HO^\bullet \rightarrow HO_2^\bullet + O_2^{\bullet -} \quad (8)$$

$$O_3^{\bullet -} + HO^\bullet \rightarrow O_3 + HO^- \quad (9)$$

$$HO^\bullet + O_3 \rightarrow HO_2^\bullet + O_2 \quad (10)$$

$$HO_2^- + H^+ \rightarrow H_2O_2 \quad (11)$$

$$H_2O_2 \leftrightarrow HO_2^- + H^+ \quad (12)$$

$$HO^\bullet + H_2O_2 \rightarrow HO_2^\bullet + H_2O \quad (13)$$

$$HO^\bullet + HO_2^- \rightarrow HO_2^\bullet + HO^- \quad (14)$$

Considering that all the single ozonation reactions (Fig. 2a) have occurred under a slightly alkaline environment, following a similar descending pH profile (Fig. SM-1a) starting at pH 8.9 (average) and ending at pH 7.6 (average), it can be concluded that both direct and

indirect pathways contributed to the organic matter degradation. This slight alteration of less than 1.5 pH units can be ascribed to the buffering capacity of leachate intrinsic bicarbonates. It should also be noted that, while the DOC removals varied from 20% to 35%, after a 3-h reaction, the degradation of aromatic compounds, estimated through the specific ultraviolet absorbance (SUVA) at 254 nm (Fig. SM-1b), was substantially higher (around 72–95%), reaching SUVA values between 1.5 and 0.2 L mg^{-1} m^{-1} (from 20 to 50 mg O_3 L^{-1}), right after 1-h reaction time. These results endorse the fact that molecular O_3 and/or reactive by-products resulting from its decomposition has the ability to promptly attack aromatic compounds and unsaturated carbon bonds, decreasing the aromatic character of the dissolved organic matter. As a result, the formed side products, such as carboxylic acids and aldehydes, are harder to mineralise [16]. Higher mineralisation degrees could likely have been achieved for longer contacting times.

3.2.2. *Effect of the H_2O_2 addition*

As previously reported, O_3 alone has been found to achieve low mineralisation levels (see Table 2), with very close DOC removal profiles when OD_{inlet} was used between 30 and 50 mg O_3 min^{-1}. Since it was not possible to significantly improve the ozonation efficiency by the increase of O_3 dosage, a strategy to optimise the overall ozonation process might involve boosting the indirect reaction mechanism, either by raising the pH (O_3/HO^-) or by adding H_2O_2 (O_3/H_2O_2) [18]. These two O_3-based AOPs generate the highly reactive $HO^\bullet$, as a result of O_3 decomposition (Eqs. (2)–(14)), which is enhanced by a sequence of radical type reactions initiated by HO^- or H_2O_2, according to the following routes [18,31,32]: (i) reaction of O_3 with HO^- to produce superoxide anions radicals ($O_2^{\bullet-}$), which undergo a series of reactions that leads to $HO^\bullet$, presenting a yield of 1 mol $HO^\bullet$ per 1.5 mol of O_3; and (ii) partial dissociation of H_2O_2 into hydroperoxide ion (HO_2^-), its conjugated base (pKa = 11.8), which quickly react with O_3 to initiate a radical chain mechanism that guides to $HO^\bullet$, rendering a yield of 1 mol $HO^\bullet$ per 1 mol of O_3. Besides the lower yield of the first approach, the increase in pH could hinder the ozonation reaction by the increase of the carbonates fraction, which are stronger $HO^\bullet$ scavengers than bicarbonates [18,32]. Beyond that, as regards the second approach, in addition to being an initiator, H_2O_2 is also a promoter, or chain carrier, of the O_3 decomposition, thus maximising the production of $HO^\bullet$ [32]. All in all, it was decided upon to follow the assays through the second approach, and the perozonation (O_3/H_2O_2) process was appraised for inlet O_3 dosages of 30, 40, and 50 mg O_3 min^{-1}.

In order to understand the influence of the H_2O_2 dosing method, two experiments using an OD_{inlet} of 30 mg O_3 min^{-1} were initially performed, in which the H_2O_2 was fed to the system: (i) periodically, by adding the required volumes to maintain its content amongst 200 and 500 mg L^{-1} throughout the 3-h reaction, as previous studies related to leachates' treatment by photochemical processes showed a good balance between the oxidation reaction rate and the oxidant consumption rate using an H_2O_2 concentration within this interval; and (ii) as a single dose right at the reaction beginning, by adding the total volume that was added in the periodic mode. The only noteworthy differences observed between these two experiments were at the level of H_2O_2 consumption and availability. When the single-dose method was used, the amount of DOC removed per gram of H_2O_2 consumed was lowered from 182 ± 9 to 127 ± 8 mg C g^{-1} H_2O_2, and H_2O_2 was depleted between the 150- and 180-min of reaction. This behaviour suggests that H_2O_2 was being consumed in parasitic reactions. Therefore, for a more efficient use of H_2O_2, periodic addition mode was chosen to pursue the trials.

As can be seen from Fig. 2a, b, d and Table 2, the addition of H_2O_2 was effectively able to provide faster DOC decays than ozonation as the O_3 content fed to the system increased, due to the extra amount of $HO^\bullet$ available to react with the organic matter, indicating that the indirect kinetic regime was indeed boosted. In fact, the integration of O_3 with H_2O_2 has led to synergies of 20 ± 2%, 30 ± 3%, and 48 ± 6% for OD_{inlet} of 30, 40, and 50 mg O_3 min^{-1}, respectively, which were estimated considering the pseudo-first-order kinetic constants for each OD_{inlet} condition, in the presence and absence of H_2O_2 (Synergy (%) = $(k_{O3/H2O2}/(k_{O3} + k_{H2O2}) - 1) \times 100$), and that the H_2O_2 alone was not responsible for any DOC removal (data not shown since there was no change on DOC values throughout 180 min). Likewise, the efficiency in terms of O_3 consumption was also improved when H_2O_2 was supplied (see Fig. 2d: inlet), and maximum O_3 concentrations of 4 mg O_3 L^{-1} were detected in the off-gas stream, while during the single ozonation trials, the outlet O_3 content has reached values of one order of magnitude higher. Accordingly, the total amount of O_3 transferred over the 3-h reaction time was also higher when H_2O_2 was added, fundamentally for OD_{inlet} of 40 and 50 mg O_3 min^{-1}. Overall, the O_3/H_2O_2 process has allowed achieving O_3 utilisation ratios above 0.99 regardless of the amount of O_3 introduced into the reaction medium, together with an enhancement of the specific relation between the carbon removed and O_3 transferred by about 10–18% (Fig. 2c and Table 2). Moreover, despite presenting similar profiles, pH decrease was slightly slower (on average, the pH decayed from 9.0 to 8.0 after a 3-h reaction time – Fig. SM-2a) when H_2O_2 was added, indicating that the organics oxidation reactions took place preferentially by the $HO^\bullet$ attack and molecular O_3 reactions were, to some extent, impaired.

Regarding the O_3/H_2O_2 process alone, it was noted that keeping H_2O_2 continuously available within a concentration range of 200–500 mg L^{-1}: (i) the H_2O_2 specific consumption was statistically not different regardless of the OD_{inlet} applied, being the quantity of DOC depleted per gram of H_2O_2 consumed in average (17 ± 2) × 10 mg C g^{-1} H_2O_2 (see Fig. 2e and Table 2); (ii) the DOC degradation rate was increased by about 25% as the OD_{inlet} was increased from 30 to 40 mg O_3 min^{-1}, with a consistent $[H_2O_2]$:$[O_3]$ molar ratio of 0.47:1 (total amount of the H_2O_2 consumed over O_3 transferred during the 3-h reaction), which is very close to an optimum molar ratio for peroxone process reported elsewhere ($[H_2O_2]$:$[O_3]$ molar ratio of 0.5:1) [33]; and (iii) the mineralisation kinetics were not affected by the increment of the OD_{inlet} from 40 to 50 mg O_3 min^{-1} and the decrement of the $[H_2O_2]$:$[O_3]$ molar ratio from 0.47:1–0.41:1 (Fig. 2b, d). These results, along with the low dissolved O_3 concentrations detected (Fig. SM-2b), suggest that for OD_{inlet} above 40 mg O_3 min^{-1}, $HO^\bullet$ generation is quenching by the O_3 in excess, possibly by the occurrence of parallel side reactions not conducting to $HO^\bullet$ production [34,35]. Despite the OD_{inlet} of 40 mg O_3 min^{-1} has provided the best performance regarding the O_3/H_2O_2 process, an OD_{inlet} of 30 mg O_3 min^{-1} was selected to evaluate the remaining experimental conditions, since it led to the most efficient results in the ozonation alone. Besides that, under this dosage, virtually no O_3 was detected in the off-gas stream and similar TOD values were obtained in spite of the H_2O_2 attendance or not.

3.2.3. *Effect of the UVC irradiation*

Another approach to potentially improve the O_3 oxidising power is to combine O_3 with UVC radiation. In an aqueous solution, the introduction of UVC photons can induce the photolysis of O_3 into H_2O_2, according to Eq. (15). Then, the newly-generated H_2O_2 can also undergo photolysis (Eq. (16)), which gives rise to the direct production of additional $HO^\bullet$, and/or, under alkaline conditions, dissociate into HO_2^-, which in turn reacts with O_3, thus initiating the radical chain mechanism by electron transfer, which can also result in the generation of free $HO^\bullet$ [29].

$$O_3 + H_2O + h\nu \rightarrow H_2O_2 + O_2 \quad (15)$$

$$H_2O_2 + h\nu \rightarrow 2\,HO^\bullet \quad (16)$$

Aiming at achieving higher synergy levels, two photo-assisted reactions were carried out, applying an OD_{inlet} of 30 mg O_3 min^{-1} at natural pH: (i) UVC-driven ozonation (O_3/UVC); and (ii) UVC-driven perozonation (O_3/H_2O_2/UVC). Furthermore, a UVC/H_2O_2 blank experiment was also performed, leading to null DOC decay along with low H_2O_2 consumption (~0.32 g L^{-1}) within a 3-h interval (Fig. 3 and

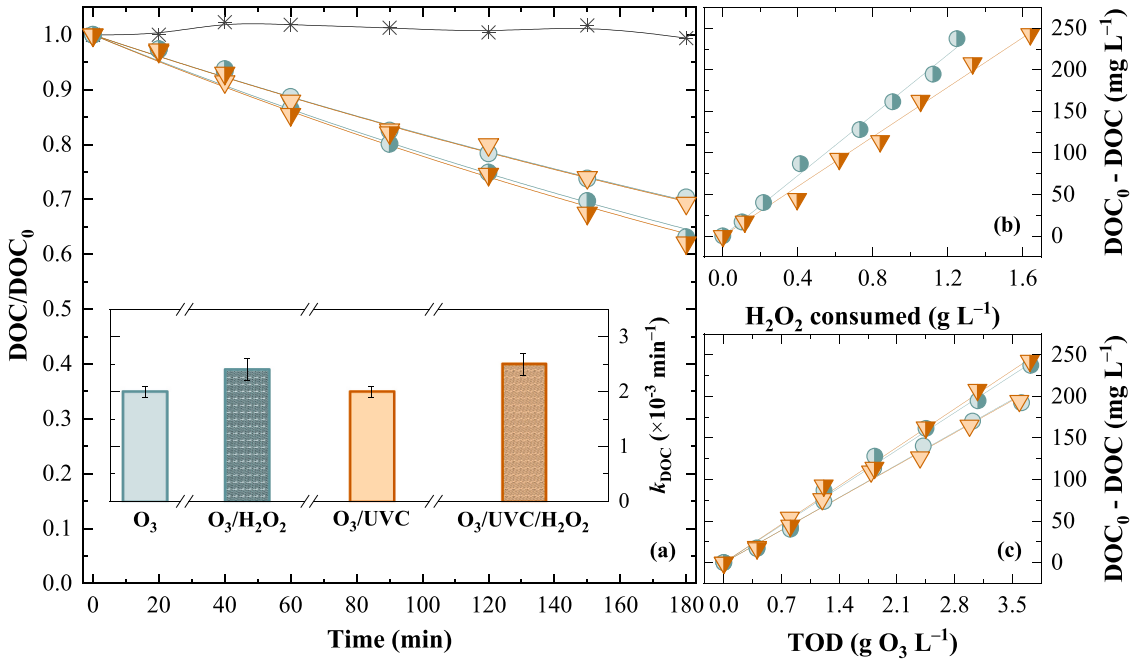

Fig. 3. Evolution of the: (a) normalised DOC reduction (symbols) over time, along with the respective pseudo-first-order fitting curves (lines); and total DOC removed as a function of the (b) H_2O_2 consumed and (c) transferred O_3 dose (TOD), during the different O_3- and/or photo-based processes: ozonation (◯), O_3/H_2O_2 (◑), O_3/UVC (▽), O_3/UVC/H_2O_2 (▼), and UVC/H_2O_2 (✳). Inset: Representation of the kinetic constants (bars) for each experiment. Experimental conditions: $[DOC]_0 = 637 \pm 24$ mg L^{-1}; $V = 1.5$ L; room temperature; $pH_0 = 8.9 \pm 0.2$; $OD_{inlet} = 30$ mg O_3 min^{-1}; $[H_2O_2] = 200$–500 mg L^{-1} (except when indicated); 11 W UVC lamp (except when indicated).

Table 2). These results suggest that neither the organic matrix was susceptible to direct photolysis nor the photolytic cleavage of H_2O_2 into two $HO^{\bullet}$ occurred in a significant way, most probably due to the extremely low UV transmissibility of the leachate (see transmittance at 254 nm - Table 1) and the presence of light-absorbing species acting as inner-filters. Notwithstanding, although in very low extent, the H_2O_2 consumption could potentially be attributed to the: (i) homolytic cleavage of the peroxide bond (–O–O–) to form $HO^{\bullet}$ (Eq. (16)); (ii) reaction of H_2O_2 with its conjugated base (Eq. (17)) [36], with no production of $HO^{\bullet}$; (iii) quenching of $HO^{\bullet}$ by reaction with H_2O_2 (Eq. (13), $k = (2.7 \pm 0.3) \times 10^7$ L mol^{-1} s^{-1}) and/or HO_2^- (Eq. (14), $k = (7.5 \pm 1.9) \times 10^9$ L mol^{-1} s^{-1}) [37]; and (iv) self-decomposition of H_2O_2 (Eq. (18)), preferentially under alkaline conditions [38].

$$HO_2^- + H_2O_2 \rightarrow H_2O + O_2 + OH^- \quad (17)$$

$$2H_2O_2 \rightarrow 2H_2O + O_2 \quad (18)$$

Contrary to the desired, the addition of UVC radiation was not able to enhance the efficiency of O_3 and O_3/H_2O_2 processes. Fig. 3a and Table 2 reveal that the kinetic constants regarding DOC degradation were statistically not different (with a confidence level of 95%) between O_3 and O_3/UVC processes and between O_3/H_2O_2 and O_3/H_2O_2/UVC processes. The same trend was found as regards the pH profile (Fig. SM-3a), and the amount of DOC removed as a function of TOD (see Fig. 3c and Table 2), with virtually no unused O_3 for all trials (Fig. SM-3b), being reached O_3 utilisation ratios between 0.96 and 0.99.

The major dissimilarity concerns the H_2O_2-assisted reactions, where it was found an H_2O_2 consumption for O_3/H_2O_2/UVC process about 29% higher than for O_3/H_2O_2 process (see Fig. 3b and Table 2), which is the equivalent to a difference of 0.36 g H_2O_2 L^{-1}. Such outcomes are in good agreement with the H_2O_2/UVC blank trial, where an H_2O_2 consumption of 0.32 g L^{-1} was noticed along with no mineralisation, suggesting the occurrence of parasitic reactions consuming H_2O_2. Therefore, the failure of the UVC light to boost the O_3 and O_3/H_2O_2 processes can potentially be ascribed to the low leachate UV-transmittance and the presence of some chromophore groups which strongly absorbed the UVC photons, thus blocking the generation of additional $HO^{\bullet}$ [29].

Accordingly, considering all these results, the different O_3-driven processes applied to the desulphurised HISWL leachate (using an OD_{inlet} of 30 mg O_3 min^{-1}) may be ordered from the least to the most efficient, in terms of mineralisation kinetic constants, as follows: ozonation ($2.0 \pm 0.1 \times 10^{-3}$ min^{-1}) ≈ O_3/UVC ($2.0 \pm 0.1 \times 10^{-3}$ min^{-1}) < O_3/H_2O_2 ($2.4 \pm 0.2 \times 10^{-3}$ min^{-1}) ≈ O_3/H_2O_2/UVC ($2.5 \pm 0.2 \times 10^{-3}$ min^{-1}).

3.2.4. *Effect of the HISWL leachate pre-treatment*

The last approach tested to upgrade ozonation and O_3-based processes was the application of an upstream coagulation process, after the sequential CO and CP stages. This additional pre-treatment aimed at the removal of part of the DOM and total suspended solids, thus increasing the transmissibility of the HISWL leachate. On the one hand, light absorption by photoactive species is enhanced, which is of the utmost importance when photo-driven reactions are intended. On the other hand, undesired competitive O_3 reactions with particulate matter are avoided, which have shown themselves to be as sharp as the ones with highly reactive DOM moieties [39]. In that way, desulphurised HISWL leachate underwent coagulation with: (i) a ferric salt at acidic medium, aiming at further Fe-catalysed- or PF-assisted ozonation (O_3/Fe^{2+} or O_3/PF); and (ii) an aluminium salt at near-neutral pH (O_3/Al^{3+}), to benefit from the alkaline pH and buffer capacity of the leachate, as well as from both direct electrophilic attack by molecular O_3 and indirect attack by $HO^{\bullet}$ resulting from O_3 decomposition. Then, the coagulated leachate was subjected to ozonation or O_3/H_2O_2/UVC processes.

Fe-driven coagulation was performed under the best conditions (100 mg Fe^{3+} L^{-1}; pH of 2.8) reported in a previous paper [10], using a leachate from the same HISWL, and Al-driven coagulation was optimised regarding the solution pH and the coagulant dosage. The best compromise in terms of DOC and turbidity removal was attained for an aluminium content of 400 mg Al^{3+} L^{-1} at free pH (Table SM-2). Regardless of the coagulant used, a DOC removal of 21–22% and a

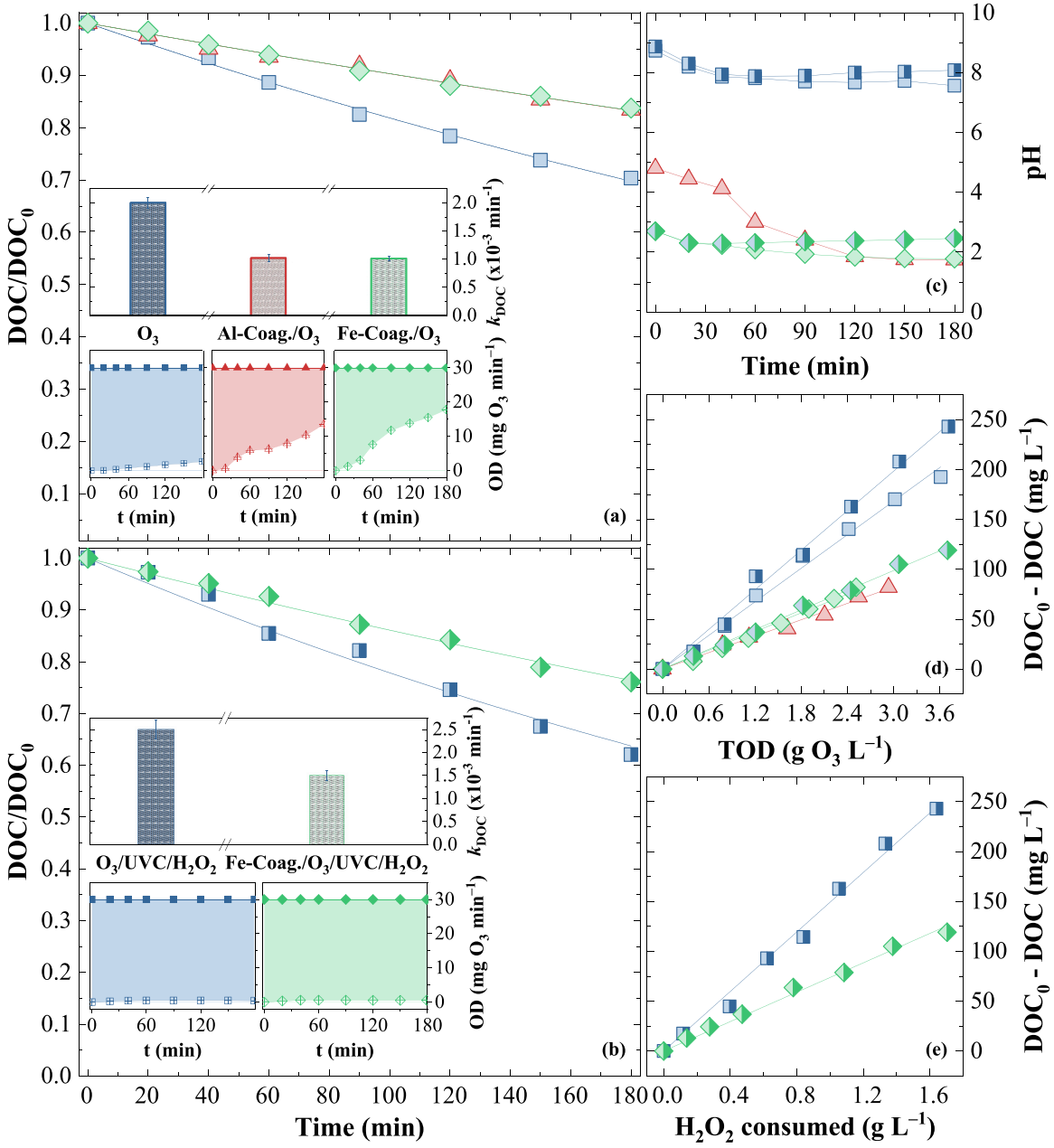

Fig. 4. Evolution of the: (a, b) normalised DOC reduction (symbols) over time, along with the respective pseudo-first-order fitting curves (lines); (c) pH over time; and total DOC removed as a function of the (d) transferred O_3 dose (TOD) and (e) H_2O_2 consumed; during the ozonation process (filled symbols), the O_3/H_2O_2 process and the $O_3/UVC/H_2O_2$ process (semi-filled symbols), using desulphurised (□,◨), Fe-coagulated (◇,◈) or Al-coagulated (△) HISWL leachate. Inset: Representation of (i) kinetic constants for each experiment and (ii) inlet (solid symbols) and outlet (crossed symbols) O_3 dose over time, where the shaded areas correspond to the total amount of O_3 available for the reaction. Experimental conditions: $[DOC]_0 = 637 \pm 24$ mg L^{-1} (desulphurised leachate) or 499 ± 6 mg L^{-1} (coagulated leachate); $V = 1.5$ L; room temperature; $OD_{inlet} = 30$ mg O_3 min^{-1}; $[H_2O_2] = 200$–500 mg L^{-1} (except when indicated); 11 W UVC lamp (except when indicated).

turbidity raise of 163–189% were obtained. Nevertheless, as anticipated, two main differences were noticed with reference to the Fe- and Al-coagulated leachate, respectively: (i) the solution pH was 2.7 against 4.8; and (ii) residual Fe (total dissolved iron) and Al (total aluminium) concentrations were 61 mg Fe L^{-1} (56 mg Fe^{2+} L^{-1} + 5 mg Fe^{3+} L^{-1}) and 6.8 mg Al L^{-1}, accompanied by an increase in the content of the respective co-anions (about more 0.500 g Cl^- L^{-1} and 2.2 g SO_4^{2-} L^{-1}). In spite of the coagulation has accounted for DOM removal, although low, the same was not valid for suspended particulate matter, even caused it to worsen. Such behaviour could be related to the molecular composition of the HISWL leachate, indicating that the main constituents of the dissolved and colloidal matter were not susceptible to the charge neutralisation mechanism and further micro-flocs aggregation, either by the preponderance of positively charged sites instead of the negative ones or by the lack of charged groups. Hence, the main goals towards the implementation of this pre-treatment were not fully achieved.

Regarding O_3-mediated reactions, Fig. 4a, b and Table 2 show that the mineralisation rates were about 40% or 49% slower when coagulated leachates were subjected to $O_3/H_2O_2/UVC$ or ozonation alone, respectively. This lower performance can conceivably be associated with the: (i) higher turbidity (53 ± 3 NTU vs. 19 ± 2 NTU); (ii) lower DOC (499 ± 6 mg L^{-1} vs. 637 ± 24 mg L^{-1}); (iii) greater concentration of chloride (20.2 g L^{-1} vs. 19.7 g L^{-1}, as a result of $FeCl_3$ addition) or sulphate (0.5 g L^{-1} vs. 2.7 g L^{-1}, as a result of $Al_2(SO_4)_3$ addition), which can act as $O_3/HO^•$ or $HO^•$ scavengers, respectively [18]; and (iv) minor pH (2.7–4.8 vs. 8.9) (see Fig. 4c); of the coagulated HISWL leachate, at

the beginning of the O_3-driven process, in contrast with the desulphurised HISWL leachate. Conducting the reaction under a considerably acidic pH range (4.8–1.7), rather than a slightly alkaline (8.9–7.6) one, dictated the prevalence of the direct O_3 reaction mechanism over the indirect one, which led to a lesser production of the powerful and non-selective $HO^{\bullet}$. As molecular O_3 presents lower redox potential than free $HO^{\bullet}$, the mineralisation kinetics was slower. These results, together with the better performance of the O_3/H_2O_2 process faced to O_3 only (showed in Section 3.2.2), might confirm that the leachate molecules, as well as the respective intermediates, are more susceptible to the attack of the $HO^{\bullet}$ than of the O_3.

Similarly to what was reported in the previous sections, the fraction of unused O_3 was higher in the absence of UVC and H_2O_2, especially whenever employed after coagulation (see Fig. 4a, b: inset). Besides that, the mineralisation efficiency in terms of O_3 or H_2O_2 consumption was about 50% lower when coagulated leachates were used, rather than the desulphurised one, whatever the remaining experimental conditions (Fig. 4d,e), suggesting the occurrence of parasitic reactions that consume O_3 and H_2O_2, either with particulate organic or soluble inorganic compounds, which impaired the degradation of the dissolved organic pollutants. In the absence of UVC light and H_2O_2, and even at a low extent, the production of $HO^{\bullet}$ as a result of O_3 decomposition could also take place in the acidic O_3/Al^{3+} and O_3/Fe^{2+} systems by the reaction with: (i) HO^-, since initial pH is higher than 4 (Fig. 4c), as shown in Section 3.2.1; and (ii) Fe^{2+}, either through the generation of O_3^- anion or through the generation of ferryl ion ($(FeO)^{2+}$) oxidant, according to Eqs. (19)–(23) [29,40].

$$Fe^{2+} + O_3 \rightarrow Fe^{3+} + O_3^- \quad (19)$$

$$O_3^- + H^+ \leftrightarrow HO_3 \quad (20)$$

$$HO_3 \rightarrow HO^{\bullet} + O_2 \quad (21)$$

$$Fe^{2+} + O_3 \rightarrow (FeO)^{2+} + O_2 \quad (22)$$

$$(FeO)^{2+} + H_2O \rightarrow Fe^{3+} + HO^{\bullet} + OH^- \quad (23)$$

In turn, contributing to the low mineralisation degrees, in the O_3/Al^{3+} and O_3/Fe^{2+} systems, the free $HO^{\bullet}$ and $HO^{\bullet}/(FeO)^{2+}$ oxidants can have been scavenged by the reaction with: (i) SO_4^{2-}, whose concentration ascended to 2.7 g L^{-1} (in contrast with 0.5 g L^{-1}), giving the radical $SO_4^{\bullet-}$ (E^o of 2.60 V/SHE), which can further react with SO_4^{2-}, to produce persulphate (E^o of 2.12 V/SHE) as stated by Eqs. (24) and (25) [18]; and (ii) Fe^{2+} (Eqs. (26) and (27)), whose concentration ranged between 56 and 42 mg L^{-1} during the reaction [29].

$$SO_4^{2-} + HO^{\bullet} \rightarrow SO_4^{\bullet-} + OH^- \quad (24)$$

$$SO_4^{2-} + SO_4^{\bullet-} \rightarrow S_2O_8^{2-} + e^- \quad (25)$$

$$HO^{\bullet} + Fe^{2+} \rightarrow Fe^{3+} + OH^- \quad (26)$$

$$(FeO)^{2+} + Fe^{2+} + 2H^+ \rightarrow 2Fe^{3+} + H_2O \quad (27)$$

Additionally, under acidic conditions and UVC light, O_3 and H_2O_2 can react with $HO^{\bullet}$ producing the less reactive perhydroxyl radical ($HO_2^{\bullet}$) (E^o of 1.70 V/SCE [29]), as displayed in Eqs. (10) and (13). Notwithstanding, for all systems considered till here (including those addressed in the previous sections), only DOC removals in the range of 16–45% were attained over a 3-h reaction time. These general low mineralisation yields might well be related to the high chloride content (>19 g Cl^- L^{-1}) of the HISWL leachate since Cl^- can quench both O_3 and $HO^{\bullet}$, according to Eq. (28) ($k = 8.9 \times 10^7$ L mol^{-1} s^{-1}) and (29) ($k = 0.003$ L mol^{-1} s^{-1}), respectively [18]. Given the continuous availability of molecular O_3, it is very plausible that chlorides quickly reappear in the solution as shown in Eq. (30) ($k = 110$ L mol^{-1} s^{-1}), once its rate constant is higher than the one of the reactions represented by Eq. (29) [18].

$$HO^{\bullet} + Cl^- \rightarrow ClOH^{\bullet-} \quad (28)$$

$$O_3 + Cl^- \rightarrow O_2 + OCl^- \quad (29)$$

$$O_3 + OCl^- \rightarrow 2O_2 + Cl^- \quad (30)$$

Looking at the single ozonation process (Fig. 4a, c), it can be observed that there was no significant difference in using Al- or Fe-coagulated leachate regarding the kinetic constants for DOC degradation ($k \approx 1 \times 10^{-3}$ min^{-1}) and final pH (1.7–1.8). Excepting O_3 concentration in the off-gas that was slightly different (Fig. 4a: inset), reaching O_3 utilisation ratios of 0.67 and 0.78 for O_3/Fe^{3+} and O_3/Al^{3+} systems. The higher consumption perceived for the second system can be explained by the higher initial pH (4.8 vs. 2.7), which apparently had more influence on the O_3 decomposition chain reactions than the presence of Fe^{2+} ion.

From Fig. 4a, b and Table 2, it was also possible to disclose that the introduction of UVC light and H_2O_2 into the O_3 reaction system led to a reaction rate improvement of (i) 25%, when Fe^{2+} was absent, and (ii) 50%, when Fe^{2+} was present. Such a tendency can be accounted for several parallel pathways capable of producing greater amounts of highly reactive species, besides the former mentioned $HO^{\bullet}$-generating reactions regarding the ozonation, O_3/H_2O_2, O_3/UVC, O_3/H_2O_2/UVC, and O_3/Fe^{2+} systems. Under the presence of Fe^{2+}, the different parallel pathways could include: (i) classical Fenton's reaction via Eq. (31) [41]; (ii) photoreduction of Fe(III)-hydroxy complexes to Fe^{2+}, according to Eq. (32) [41]; (iii) direct photolysis of Fe(III)-carboxylate complexes as stated by the general Eq. (33) [42]; and (vi) reaction of resulting Fe^{3+} with O_3, in line with Eq. (34) [29]. Furthermore, aside from Eqs. (32) and (33), Fe^{2+} could also be regenerated from the chemical reduction of Fe^{3+} with H_2O_2 and $HO_2^{\bullet}$, even to a low extent, conforming to Eqs. (35) and (36) [43]. So, continuous generation of $HO^{\bullet}$ could be maximised by the occurrence of the reactions (32) and (33), and (35) and (36) that guarantee the catalytic loop of the Fe^{3+}/Fe^{2+}, allowing a Fe^{2+} content enough to propagate the reactions (19)–(23) and (31).

$$Fe^{2+} + H_2O_2 \rightarrow Fe^{3+} + HO^{\bullet} + OH^- \quad (31)$$

$$FeOH^{2+} + h\nu \rightarrow Fe^{2+} + HO^{\bullet} \quad (32)$$

$$Fe^{3+}(L)_n + h\nu \rightarrow Fe^{2+}(L)_{n-1} + L_{ox}^{\bullet} \quad (33)$$

$$Fe^{3+} + O_3 \rightarrow (FeO)^{2+} + H^+ + O_2 + HO^{\bullet} \quad (34)$$

$$Fe^{3+} + H_2O_2 \rightarrow Fe^{2+} + H^+ + HO_2^{\bullet} \quad (35)$$

$$Fe^{3+} + HO_2^{\bullet} \rightarrow Fe^{2+} + H^+ + O_2 \quad (36)$$

Also, the slower decrease in pH for O_3/PF than for O_3/Fe^{2+} system supports the fact that this leachate is preferentiality attacked by free $HO^{\bullet}$ instead of the O_3 molecular. It is worthy of mentioning that a blank UVC/H_2O_2 experiment using the Fe-coagulated HISWL leachate (see Table 2) at an average pH of 2.8, the so-called PF reaction, was also performed, showing a DOC removal rate 40% and 59% lower than the O_3/Fe^{2+} and O_3/PF processes under the same conditions. Although a quicker organics removal had been achieved, synergy was not accomplished by the integrated O_3/PF system, as its kinetic constant was lower than the sum of the kinetic constants for the individual O_3/Fe^{2+} and PF processes, as shown in Table 2.

As a final remark, it was found that even though higher reaction rates were reached for O_3-based systems using the HISWL leachate right after the CO and CP stages, in absolute terms, the DOC reduction was higher when the desulphurised HISWL leachate undergone treatment by coagulation combined with O_3-based processes (34% or 40% vs. 30% or 38% for O_3/Fe^{2+} or O_3/PF vs. ozonation or O_3/H_2O_2/UVC,

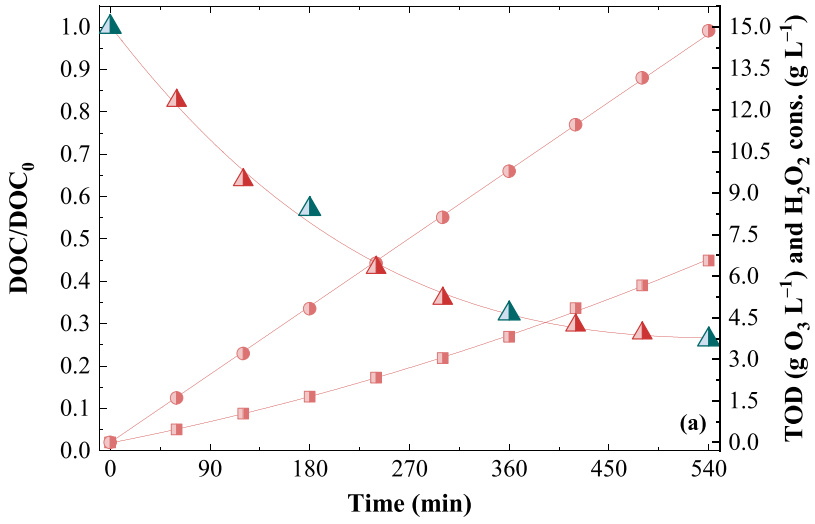

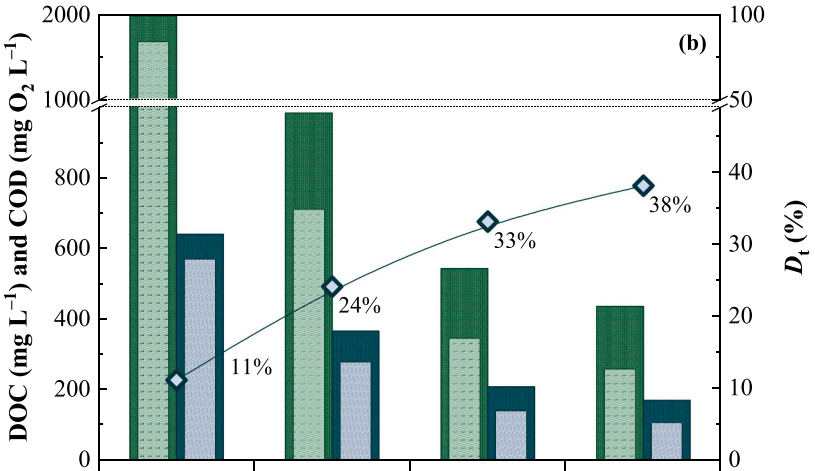

	0 min	180 min	360 min	540 min
DOC (day 0)	637	363	206	167
DOC (day 28)	567	276	138	104
COD (day 0)	1970	980	540	433
COD (day 28)	1667	708	343	256

Fig. 5. Evolution of the: (a) normalised DOC reduction (▲,▲), whose the symbols highlighted in green correspond to the samples submitted to the Zahn-Wellens test, transferred O_3 dose (TOD) (●) and H_2O_2 consumed (■) over time, during the treatment of desulphurised HISWL leachate by O_3/H_2O_2 process; and (b) DOC and COD at day 0 and 28 (bars) of the Zahn-Wellens test, as well as the biodegradation percentage at day 28 (symbols), considering the samples collected at 0, 180, 360 and 540 min of the O_3/H_2O_2 process. Experimental conditions: $[DOC]_0 = 637 \pm 24$ mg L^{-1}; $V = 1.5$ L; room temperature; $pH_0 = 8.9 \pm 0.2$; $OD_{inlet} = 40$ mg O_3 min^{-1}; $[H_2O_2] =$ 200–500 mg L^{-1}.

respectively). However, the inclusion of a coagulation stage would also imply the addition of another neutralisation step after the O_3-driven process. So, it was decided to exclude the coagulation from the treatment line and pursue the biodegradability assessment using desulphurised HISWL leachate along the O_3/H_2O_2 process under an OD_{inlet} of 40 mg O_3 min^{-1}, since it was the condition that provided the best results in terms of contaminants removal.

3.2.5. Biodegradability assessment

One of the most important indicators to appraise the effectiveness of O_3-based systems, especially when treating high-polluted wastewater whose total mineralisation is too difficult and economically not viable, is the biodegradability enhancement along the reaction. In order to attest to the applicability of a biological oxidation process downstream from the O_3-based AOP and define the best organics oxidation state to end it, the Zahn-Wellens test was performed on samples collected at 0-, 3-, 6- and 9-h of the O_3/H_2O_2 process with an OD_{inlet} of 40 mg O_3 min^{-1} (Fig. 5). The overall purpose is cost reduction, which means that the O_3/H_2O_2 process should be as short as possible and yet sufficient to help the biological oxidation process to reach the legal discharge requirements, especially in terms of COD levels.

As expected, the ozonation reaction promotes a progressive enhancement in the biodegradation rate (D_t) from 11%, at time 0, up to 38%, after a 9-h reaction, which is equivalent to an O_3 dose of 14.9 g L^{-1} leachate and an H_2O_2 consumption of 6.6 g L^{-1} leachate (Fig. 5). Nevertheless, to achieved COD values below 125 mg O_2 L^{-1} (European legislation) or 150 mg O_2 L^{-1} (Portuguese legislation) after biological oxidation, it would be necessary to carry out the O_3/H_2O_2 process for more than 9-h, which is not economically feasible. In fact, the preliminary unitary operating cost assigned only to O_3/H_2O_2 stage was estimated at 40.4 € m^{-3}, considering the: (i) total O_3 dose (14.9 g L^{-1}) and H_2O_2 consumption (6.6 g L^{-1}) after a 9-h contacting time; (ii) O_3 energy consumption and electric energy price (15 kWh kg^{-1} O_3 [20] and 0.10 € kWh^{-1}, the average market price for industrial consumers); (iii) cost related to the O_2 flow rate (15 L h^{-1}) fed to the O_3 generator (0.14 € m^{-3}, the market price of a Portuguese company); and (iv) price of an

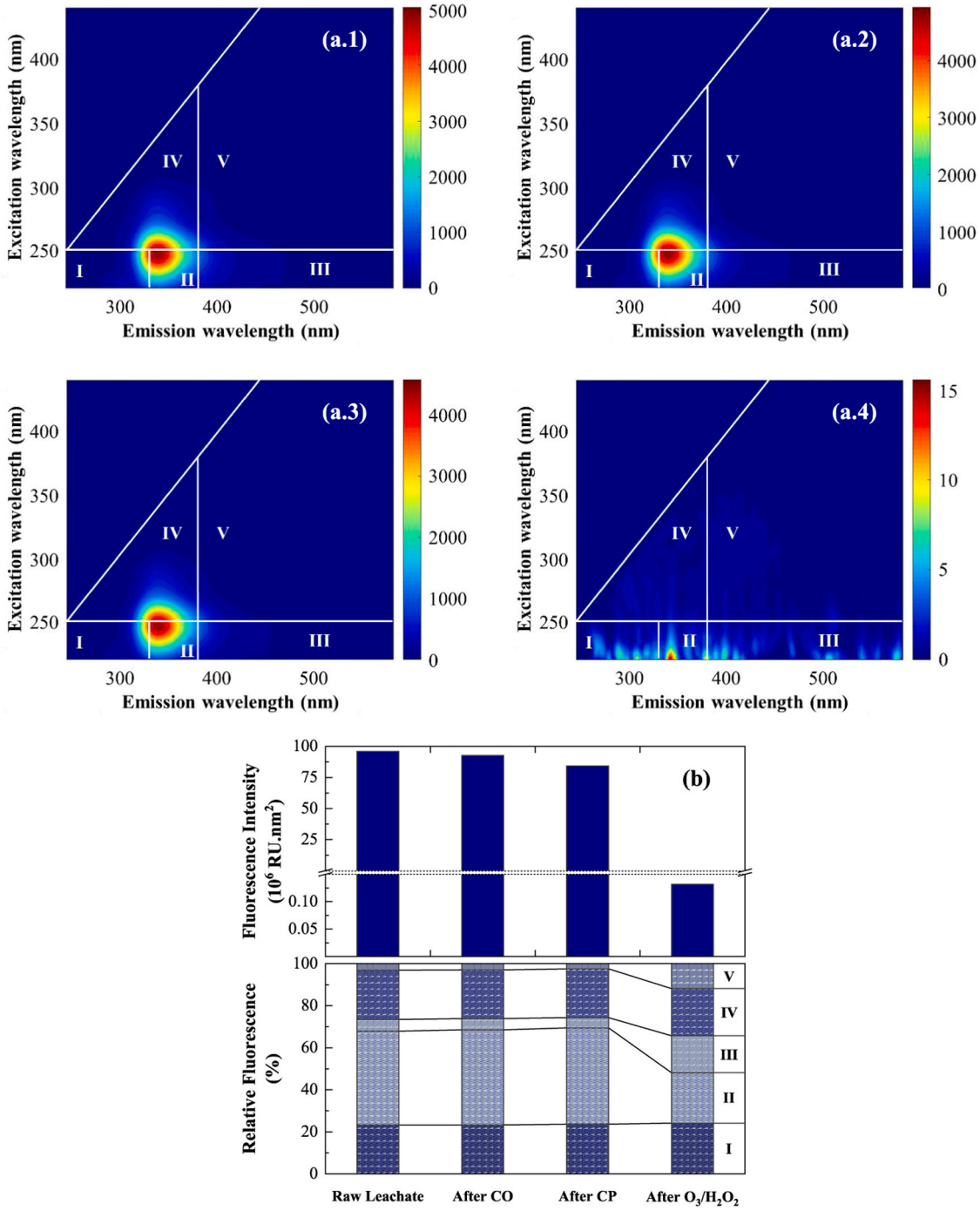

Fig. 6. Illustration of the (a) 3D-EEM spectra for (0.1) raw HISWL leachate and for HISWL leachate after (0.2) catalytic oxidation (CO), (0.3) chemical precipitation (CP) and (0.4) O_3/H_2O_2 process ($[DOC]_0 = 637 \pm 24$ mg L^{-1}, $V = 1.5$ L, room temperature, $pH_0 = 8.9 \pm 0.2$, $OD_{inlet} = 40$ mg O_3 min^{-1}, $[H_2O_2] = 200–500$ mg L^{-1}, 3-h contacting time), as well as the (b) total fluorescence intensity and relative fluorescence by region.

H_2O_2 solution at 50% (w/v) (375 € ton^{-1}, the market price of a Portuguese company).

In view of the high operating costs associated with the O_3/H_2O_2 process, when the discharge of the HISWL leachate into aquatic systems is aimed, a second approach can be its discharge into the municipal sewerage system, whose emission limited value for COD is usually 1000 mg O_2 L^{-1} (WWTP management requirement). Given this alternative, and based on the Zahn-Wellens test profile together with O_3/H_2O_2 experiment results (see Fig. 5), it was estimated that the O_3/H_2O_2 process should be carried out until an O_3 dose of 3.5 g O_3 per litre of leachate is attained and 1.1 g of H_2O_2 per litre of leachate is consumed (which corresponds to a 2.1-h reaction in this experimental facility), considering initial DOC and COD concentrations of 637 mg L^{-1} and 1970 mg O_2 L^{-1}, respectively. Under these conditions, the HISWL leachate should present a DOC and COD of (i) 433 mg L^{-1} and 1250 mg O_2 L^{-1}, respectively, after the O_3/H_2O_2 process, which means a substantially lower unitary operating cost of 9.1 € m^{-3} for O_3 stage; and (ii) 354 mg L^{-1} and 978 mg O_2 L^{-1}, respectively, after the subsequent biological oxidation process.

3.3. Dissolved organic matter characterisation

To better understand the structural and compositional changes of the DOM in the HISWL leachate throughout the best treatment train, 3D-EEM and SEC-OCD analyses were performed (as reported elsewhere [44–46]) on the following samples: (i) raw leachate; (ii) leachate after CO; (iii) leachate after CP; and (iv) leachate after O_3/H_2O_2 process (OD_{inlet} of 40 mg O_3 L^{-1}; contacting time of 3-h) (Fig. 6).

Three-dimensional EEM fluorescence spectra were divided into five regions (see Fig. 6a) based on the classification adopted by Chen et al. [44] regarding the type and location of the fluorescent material, namely: (i) region I, comprising tyrosine-like aromatic proteins (Ex < 250 nm, Em < 330 nm); (ii) region II, encompassing tryptophan-like aromatic proteins (Ex < 250 nm, 330 nm < Em < 380 nm); (iii) region III, containing fulvic acid-like matter (Ex < 250 nm, Em > 380 nm); (iv) region IV, covering soluble microbial metabolic products (Ex > 250 nm, Em < 380 nm); and (v) region V, consisting of humic acid-like matter (Ex > 250 nm, Em > 380 nm). Regionally integrated fluorescence intensities at each region and their total fluorescence intensity are depicted in Fig. 6b. In general, MSWL leachates contain recalcitrant humic acid-like and fulvic acid-like fluorophores whose fluorescent intensities are comparable with other fractions of fluorophores [47,48]. In contrast, the raw HISWL leachate consists primarily of tryptophan-like (45%), tyrosine-like (23%) aromatic proteins, and soluble microbial metabolic products (23%) (Fig. 6b), which accounts for >90% of the fluorophores. While a slight reduction in the total fluorescence intensity throughout the CO and CP stages was observed, the compositional changes of fluorophores were minimal (Fig. 6b). This observation suggests that CO and CP are non-selective for the attenuation of fluorophores. Such performance was in agreement with the treatment strategy since it was expected that CO and CP stages have a meaningful impact on the inorganic sulphur compounds and not on the DOM composition.

Interestingly, the HISWL leachate was still bio-recalcitrant despite the relatively low content of recalcitrant humic acid-like and fulvic acid-like fluorophores (i.e., <10% of the total fluorescence). Only 11–12% of the DOM was biodegradable, suggesting the presence of recalcitrant non-fluorescent DOM. Also, the inhibition of biodegradability by inorganic compounds other than sulphur compounds is plausible. Compositional characteristics of major fluorophores at regions I, II, and IV can also explain the recalcitrance. Region II is associated with heterocyclic nitrogen-containing compounds (e.g., indole) that are bio-recalcitrant. Various recalcitrant fractions such as lignin-derived polyphenolic compounds, DNA fragments, organic acids, and benzene derivatives are related to regions I and IV, which could render the leachate recalcitrant [49,50]. Furthermore, the previous volatile organic carbon analysis for the same HISWL can bolster the predominance of fluorophores at the regions I, II, and IV [11]. This might be ascribed to the type of waste deposited in the landfill, which includes sludge from MWWTPs, soils containing heavy hydrocarbons, and residues from steelworks and mining and metallurgical industries.

The SEC-OCD chromatograms support the results of 3D-EEM (Fig. 7a). The significant fractions of organic carbons (i.e., 97.1–99.2% of the total area of chromatogram) were separated at the retention time of 73.9–75.0 min, where humic substances and low molecular weight (LMW) fractions are eluted [51]. The contribution of biopolymer fractions to the organic carbon content was minimal (i.e., 0.8–2.8% of the total area). The major chromatographic peak was distributed from 40 min to 160 min, where various molecular weight fractions fall. The applied deconvolution algorithm allows clearer speciation of the organic matter. Two chromatographic components were obtained from the deconvolution: humic substances (Component 1) and LMW organic matter (Component 2), such as building blocks and LMW acids (Fig. SM-4). About five times greater peak area of LMW fractions than humic substances agrees with the fluorescence analysis in that humic substances are a minor fraction (Fig. 7b). The humic substance fraction was effectively recalcitrant by CO (i.e., ~11% removal) while being removed effectively by CP (i.e., ~40% removal). The humic removal efficacy could be attributed to its coprecipitation with barite during CO [52]. In contrast, LMW fractions were more effectively removed in CO than CP, which agrees with another study regarding the reactivity of LMW fractions in oxidation [53]. A slight increase in the peak area of Component 2 after CP might be attributed to either intramolecular rearrangement or alteration of ionic strength change that can result in conformational change. In any case, the predominance of LMW substances in the desulphurised HISWL is in accordance with the low DOC decays (20–21%) observed for the coagulation process.

The best performing O_3/H_2O_2 system drastically decreased both fluorescence intensity (>99.8%) and total SEC-OCD area (>99.5%), as shown in Figs. 6 and 7. Regarding the remaining fluorescent DOM, it is possible to infer that the physicochemical characteristics of the ozonised HISWL leachate (Fig. 6a.4) have obviously diverged from those of the

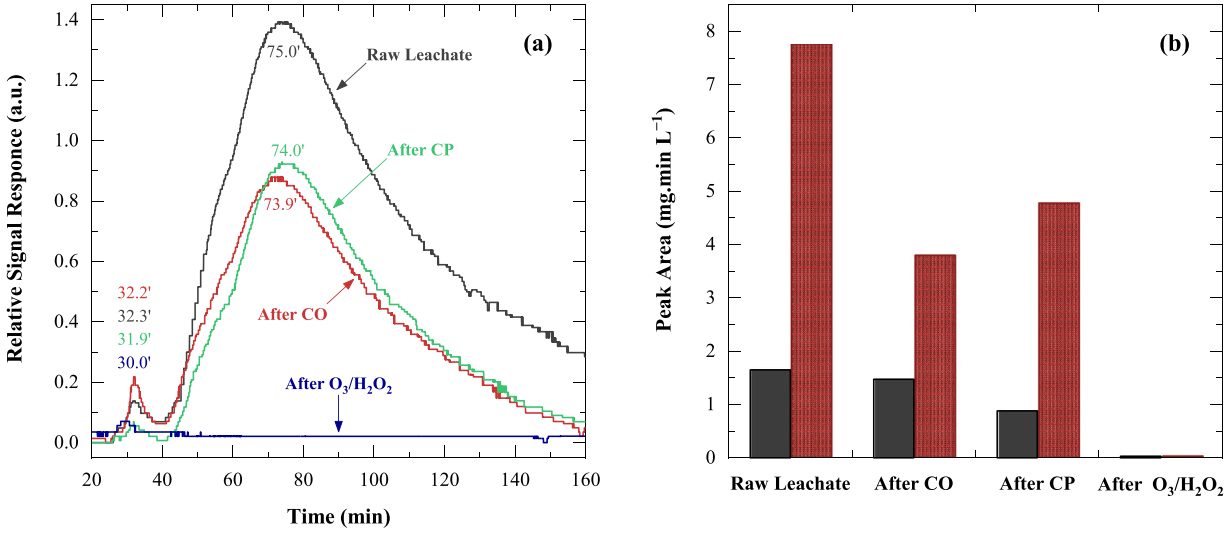

Fig. 7. (a) SEC-OCD chromatograms for raw HISWL leachate and for HISWL leachate after catalytic oxidation (CO), chemical precipitation (CP) and O_3/H_2O_2 process ($[DOC]_0$ = 637 ± 24 mg L^{-1}, V = 1.5 L, room temperature, pH_0 = 8.9 ± 0.2, OD_{inlet} = 40 mg O_3 min^{-1}, $[H_2O_2]$ = 200–500 mg L^{-1}, 3-h contacting time), as well as (b) peak area of the deconvoluted SEC-OCD components, namely: humic substances (component 1 –) and low molecular weight (LMW) substances (component 2 –).

desulphurised one (Fig. 6a.3). The considerable fluorescence reduction in O_3/H_2O_2 was partly attributed to the effective alteration of the intersystem crossing efficiency by molecular ozone [54]. Also, the high removal of SEC-OCD peak area indicates the effectiveness of O_3/H_2O_2 for mineralisation. It is noteworthy that DOC still has a noticeable concentration after O_3/H_2O_2, which was not captured by SEC-OCD. This discrepancy might be possible because O_3/H_2O_2 could generate small organic molecules out of the separation range of the SEC column. Lastly, the DOM profile of the treated HISWL leachate supported its low bioavailability, as the improvement of biodegradability during 3-h contact time in O_3/H_2O_2 was marginal (24%, Fig. 5).

4. Conclusions

The best treatment strategy to de-pollute a high-strength HISWL leachate, mainly presenting high sulphur content, moderate organic load, moderate-to-low nitrogen level, and low biodegradability, should comprise the following processes: (i) catalytic oxidation of sulphites and sulphides at natural pH using H_2O_2 as oxidant (H_2O_2:SO_3^{2-} and [H_2O_2]:[S^{2-}] molar ratios of 1:1 and 4:1, respectively) and leachate transition metals as catalysts, with the partial formation of sulphate (~33%); (ii) chemical precipitation of sulphates as barite mineral ($BaSO_4$) without pH correction and stoichiometric conditions; (iii) O_3/H_2O_2 for 2.1 h under free pH, being transferred about 3.5 kg O_3 per m^3 leachate and consumed ca. 1.1 kg H_2O_2 per m^3 leachate (associated unitary operating cost of 9.1 € m^{-3}), in order to degrade the recalcitrant organics while enhancing the biodegradability (even though at a low extent); and (iv) biological oxidation to remove the biodegradable organics fraction resulting from the O_3/H_2O_2. The application of this treatment line would allow attaining an effluent in full compliance with the WWTP management requirement for the discharge of industrial wastewater into the sewerage system, but not with Portuguese and European legislation targeting the discharge of wastewaters into water bodies. The DOM distribution in the hazardous leachate matrix obtained by the 3D-EEM and SEC-OCD analysis was found to be in agreement with the multistage treatment strategy performed, being the O_3-based AOPs step the one which had more influence on the DOM composition changes. Also, the prevalence of low molecular weight matter might justify the low performance spotted for the coagulation process. Finally, it was also established that neither the addition of UVC irradiation nor a preliminary coagulation step (likely influenced by the barium chloride addition upstream) had a positive effect on O_3-based reactions.

CRediT authorship contribution statement

Inalmar D. Barbosa Segundo: Investigation, Validation. **Ana I. Gomes:** Writing - review & editing. **Bianca M. Souza-Chaves:** Resources, Writing - review & editing. **Minkyu Park:** Resources, Writing - review & editing. **André B. dos Santos:** Writing - review & editing. **Rui A.R. Boaventura:** Writing - review & editing. **Francisca C. Moreira:** Conceptualization, Methodology, Supervision, Writing - review & editing. **Tânia F.C.V. Silva:** Conceptualization, Methodology, Supervision, Visualization, Writing - original draft, Writing - review & editing. **Vítor J.P. Vilar:** Conceptualization, Methodology, Supervision, Writing - review & editing.

Declaration of Competing Interest

The authors declare that they have no known competing financial interests or personal relationships that could have appeared to influence the work reported in this paper.

Acknowledgements

The current work had financial support from: (i) Project AIProcMat@N2020 - Advanced Industrial Processes and Materials for a Sustainable Northern Region of Portugal 2020, with the reference NORTE-01-0145-FEDER-000006, supported by Norte Portugal Regional Operational Programme (NORTE 2020), under the Portugal 2020 Partnership Agreement, through the European Regional Development Fund (ERDF); and (ii) Base Funding - UIDB/50020/2020 of the Associate Laboratory LSRE-LCM - funded by national funds through FCT/MCTES (PIDDAC). Inalmar D. Barbosa Segundo and Ana I. Gomes also want to acknowledge for their doctoral fellowship (references 205715/2014-1 and PD/BD/105980/2014), supported by the CNPq and FCT, respectively. Bianca M. Souza-chaves gratefully acknowledges her post-doctoral scholarship supported by CNPq through the Science Without Borders Program (process no. 201989/2014-0). Vítor J.P. Vilar, Tânia F. C.V. Silva and Francisca C. Moreira acknowledge the FCT Individual Call to Scientific Employment Stimulus 2017 (CEECIND/01317/2017, CEECIND/01386/2017 and CEECIND/02196/2017, respectively).

Appendix A. Supporting information

Supplementary data associated with this article can be found in the online version at doi:10.1016/j.jece.2021.105554.

References

[1] C. Pavelka, R.C. Loehr, B. Haikola, Hazardous waste landfill leachate characteristics, Waste Manag. 13 (1993) 573–580, https://doi.org/10.1016/0956-053X(93)90017-Q.
[2] A.Ž. Gotvajn, T. Tišler, J. Zagorc-Končan, Comparison of different treatment strategies for industrial landfill leachate, J. Hazard. Mater. 162 (2009) 1446–1456, https://doi.org/10.1016/j.jhazmat.2008.06.037.
[3] T.F.C.V. Silva, P.A. Soares, D.R. Manenti, A. Fonseca, I. Saraiva, R.A.R. Boaventura, V.J.P. Vilar, An innovative multistage treatment system for sanitary landfill leachate depuration: studies at pilot-scale, Sci. Total Environ. 576 (2017) 99–117, https://doi.org/10.1016/j.scitotenv.2016.10.058.
[4] M. Peyravi, M. Jahanshahi, M. Alimoradi, E. Ganjian, Old landfill leachate treatment through multistage process: membrane adsorption bioreactor and nanofitration, Bioprocess Biosyst. Eng. 39 (2016) 1803–1816, https://doi.org/10.1007/s00449-016-1655-0.
[5] E. Torres-Socías, L. Prieto-Rodríguez, A. Zapata, I. Fernández-Calderero, I. Oller, S. Malato, Detailed treatment line for a specific landfill leachate remediation. Brief economic assessment, Chem. Eng. J. 261 (2015) 60–66, https://doi.org/10.1016/j.cej.2014.02.103.
[6] A. Anfruns, J. Gabarró, R. Gonzalez-Olmos, S. Puig, M.D. Balaguer, J. Colprim, Coupling anammox and advanced oxidation-based technologies for mature landfill leachate treatment, J. Hazard. Mater. 258–259 (2013) 27–34, https://doi.org/10.1016/j.jhazmat.2013.04.027.
[7] J.-S. Guo, A.A. Abbas, Y.-P. Chen, Z.-P. Liu, F. Fang, P. Chen, Treatment of landfill leachate using a combined stripping, Fenton, SBR, and coagulation process, J. Hazard. Mater. 178 (2010) 699–705, https://doi.org/10.1016/j.jhazmat.2010.01.144.
[8] F.C. Moreira, J. Soler, A. Fonseca, I. Saraiva, R.A.R. Boaventura, E. Brillas, V.J. P. Vilar, Incorporation of electrochemical advanced oxidation processes in a multistage treatment system for sanitary landfill leachate, Water Res. 81 (2015) 375–387, https://doi.org/10.1016/j.watres.2015.05.036.
[9] A.I. Gomes, T.F. Soares, T.F.C.V. Silva, R.A.R. Boaventura, V.J.P. Vilar, Ozone-driven processes for mature urban landfill leachate treatment: organic matter degradation, biodegradability enhancement and treatment costs for different reactors configuration, Sci. Total Environ. 724 (2020), 138083, https://doi.org/10.1016/j.scitotenv.2020.138083.
[10] I.D. Barbosa Segundo, F.C. Moreira, T.F.C.V. Silva, A.D. Webler, R.A. R. Boaventura, V.J.P. Vilar, Development of a treatment train for the remediation of a hazardous industrial waste landfill leachate: a big challenge, Sci. Total Environ. 741 (2020), 140165, https://doi.org/10.1016/j.scitotenv.2020.140165.
[11] I.D. Barbosa Segundo, T.F.C.V. Silva, F.C. Moreira, G.V. Silva, R.A.R. Boaventura, V.J.P. Vilar, Sulphur compounds removal from an industrial landfill leachate by catalytic oxidation and chemical precipitation: from a hazardous effluent to a value-added product, Sci. Total Environ. 655 (2019) 1249–1260, https://doi.org/10.1016/j.scitotenv.2018.11.274.
[12] A.D. Webler, F.C. Moreira, M.W.C. Dezotti, C.F. Mahler, I.D. Barbosa Segundo, R.A. R. Boaventura, V.J.P. Vilar, Development of an integrated treatment strategy for a leather tannery landfill leachate, Waste Manag. 89 (2019) 114–128, https://doi.org/10.1016/j.wasman.2019.03.066.
[13] L. Di Palma, P. Ferrantelli, C. Merli, E. Petrucci, Treatment of industrial landfill leachate by means of evaporation and reverse osmosis, Waste Manag. 22 (2002) 951–955, https://doi.org/10.1016/S0956-053X(02)00079-X.
[14] P. Haapea, S. Korhonen, T. Tuhkanen, Treatment of industrial landfill leachates by chemical and biological methods: ozonation, ozonation + hydrogen peroxide, hydrogen peroxide and biological post-treatment for ozonated water, Ozone Sci. Eng. 24 (2002) 369–378, https://doi.org/10.1080/01919510208901627.

[15] E. Kattel, A. Kivi, K. Klein, T. Tenno, N. Dulova, M. Trapido, Hazardous waste landfill leachate treatment by combined chemical and biological techniques, Desalin. Water Treat. 57 (2016) 13236–13245, https://doi.org/10.1080/19443994.2015.1057539.

[16] S. Cortez, P. Teixeira, R. Oliveira, M. Mota, Ozonation as polishing treatment of mature landfill leachate, J. Hazard. Mater. 182 (2010) 730–734, https://doi.org/10.1016/j.jhazmat.2010.06.095.

[17] S. Cortez, P. Teixeira, R. Oliveira, M. Mota, Evaluation of Fenton and ozone-based advanced oxidation processes as mature landfill leachate pre-treatments, J. Environ. Manag. 92 (2011) 749–755, https://doi.org/10.1016/j.jenvman.2010.10.035.

[18] C. Tizaoui, L. Bouselmi, L. Mansouri, A. Ghrabi, Landfill leachate treatment with ozone and ozone/hydrogen peroxide systems, J. Hazard. Mater. 140 (2007) 316–324, https://doi.org/10.1016/j.jhazmat.2006.09.023.

[19] F.C. Moreira, E. Bocos, A.G.F. Faria, J.B.L. Pereira, C.P. Fonte, R.J. Santos, J.C. B. Lopes, M.M. Dias, M.A. Sanromán, M. Pazos, R.A.R. Boaventura, V.J.P. Vilar, Selecting the best piping arrangement for scaling-up an annular channel reactor: an experimental and computational fluid dynamics study, Sci. Total Environ. 667 (2019) 821–832, https://doi.org/10.1016/j.scitotenv.2019.02.260.

[20] A.C. Twort, D.D. Ratnayaka, M.J. Brandt. Water Supply, fifth ed., IWA Publishing, London, 2000.

[21] J. Hoigné, The chemistry of ozone in water, in: S. Stucki (Ed.), Process Technologies for Water Treatment, Springer US, Boston, MA, 1988, pp. 121–141.

[22] J. Hoigné, H. Bader, W.R. Haag, J. Staehelin, Rate constants of reactions of ozone with organic and inorganic compounds in water—III. Inorganic compounds and radicals, Water Res. 19 (1985) 993–1004, https://doi.org/10.1016/0043-1354(85)90368-9.

[23] M.H. Gerardi, Nitrification and Denitrification in the Activated Sludge Process, John Wiley & Sons, New York, 2002.

[24] P.N.L. Lens, A. Visser, A.J.H. Janssen, L.W.H. Pol, G. Lettinga, Biotechnological treatment of sulfate-rich wastewaters, Crit. Rev. Environ. Sci. Technol. 28 (1998) 41–88, https://doi.org/10.1080/10643389891254160.

[25] M.R. Hoffmann, Kinetics and mechanism of oxidation of hydrogen sulfide by hydrogen peroxide in acidic solution, Environ. Sci. Technol. 11 (1977) 61–66, https://doi.org/10.1021/es60124a004.

[26] J. Lagrange, C. Pallares, G. Wenger, P. Lagrange, Kinetics of sulphur(IV) oxidation by hydrogen peroxide in basic aqueous solution, Atmos. Environ. 30 (1996) 1013–1018, https://doi.org/10.1016/1352-2310(95)00422-X.

[27] M. Moslemi, S.H. Davies, S.J. Masten, Ozone mass transfer in a recirculating loop semibatch reactor operated at high pressure, J. Adv. Oxid. Technol. 13 (2010) 79–88, https://doi.org/10.1515/jaots-2010-0111.

[28] X. Quan, D. Luo, J. Wu, R. Li, W. Cheng, Ge s, Ozonation of acid red 18 wastewater using O_3/Ca(OH)$_2$ system in a micro bubble gas-liquid reactor, J. Environ. Chem. Eng. 5 (2017) 283–291, https://doi.org/10.1016/j.jece.2016.12.007.

[29] K. Chandrasekara Pillai, T.O. Kwon, I.S. Moon, Degradation of wastewater from terephthalic acid manufacturing process by ozonation catalyzed with Fe^{2+}, H_2O_2 and UV light: direct versus indirect ozonation reactions, Appl. Catal. B 91 (2009) 319–328, https://doi.org/10.1016/j.apcatb.2009.05.040.

[30] J. Hoigné, H. Bader, Rate constants of reactions of ozone with organic and inorganic compounds in water—II: dissociating organic compounds, Water Res. 17 (1983) 185–194, https://doi.org/10.1016/0043-1354(83)90099-4.

[31] J. Staehelin, J. Hoigne, Decomposition of ozone in water: rate of initiation by hydroxide ions and hydrogen peroxide, Environ. Sci. Technol. 16 (1982) 676–681, https://doi.org/10.1021/es00104a009.

[32] D. Gardoni, A. Vailati, R. Canziani, Decay of ozone in water: a review, Ozone Sci. Eng. 34 (2012) 233–242, https://doi.org/10.1080/01919512.2012.686354.

[33] D.B. Miklos, C. Remy, M. Jekel, K.G. Linden, J.E. Drewes, U. Hübner, Evaluation of advanced oxidation processes for water and wastewater treatment–a critical review, Water Res. 139 (2018) 118–131, https://doi.org/10.1016/j.watres.2018.03.042.

[34] A. Cruz-Alcalde, S. Esplugas, C. Sans, Continuous versus single H_2O_2 addition in peroxone process: performance improvement and modelling in wastewater effluents, J. Hazard. Mater. 387 (2020), 121993, https://doi.org/10.1016/j.jhazmat.2019.121993.

[35] S. Naumov, G. Mark, A. Jarocki, C. von Sonntag, The reactions of nitrite ion with ozone in aqueous solution – new experimental data and quantum-chemical considerations, Ozone Sci. Eng. 32 (2010) 430–434, https://doi.org/10.1080/01919512.2010.522960.

[36] F.J. Beltrán, M. González, J.F. González, Industrial wastewater advanced oxidation. Part 1. UV radiation in the presence and absence of hydrogen peroxide, Water Res. 31 (1997) 2405–2414, https://doi.org/10.1016/S0043-1354(97)00077-8.

[37] H. Christensen, K. Sehested, H. Corfitzen, Reactions of hydroxyl radicals with hydrogen peroxide at ambient and elevated temperatures, J. Phys. Chem. 86 (1982) 1588–1590, https://doi.org/10.1021/j100206a023.

[38] W.D. Nicoll, A.F. Smith, Stability of dilute alkaline solutions of hydrogen peroxide, Ind. Eng. Chem. 47 (1955) 2548–2554, https://doi.org/10.1021/ie50552a051.

[39] I. Zucker, Y. Lester, D. Avisar, U. Hübner, M. Jekel, Y. Weinberger, H. Mamane, Influence of wastewater particles on ozone degradation of trace organic contaminants, Environ. Sci. Technol. 49 (2015) 301–308, https://doi.org/10.1021/es504314t.

[40] B. Legube, N.K.V. Leitner, Catalytic ozonation: a promising advanced oxidation technology for water treatment, Catal. Today 53 (1999) 61–72, https://doi.org/10.1016/S0920-5861(99)00103-0.

[41] Y. Sun, J.J. Pignatello, Photochemical reactions involved in the total mineralization of 2,4-D by Fe^{3+}/H_2O_2/UV, Environ. Sci. Technol. 27 (1993) 304–310, https://doi.org/10.1021/es00039a010.

[42] O. Horváth, K.L. Stevenson. Charge Transfer Photochemistry of Coordination Compounds, first ed., Wiley, New York, 1992.

[43] E. Brillas, P.-Ls Cabot, R.Ma Rodríguez, C. Arias, J.A. Garrido, R. Oliver, Degradation of the herbicide 2,4-DP by catalyzed ozonation using the O_3/Fe^{2+}/UVA system, Appl. Catal. B 51 (2004) 117–127, https://doi.org/10.1016/j.apcatb.2004.02.007.

[44] W. Chen, P. Westerhoff, J.A. Leenheer, K. Booksh, Fluorescence excitation–emission matrix regional integration to quantify spectra for dissolved organic matter, Environ. Sci. Technol. 37 (2003) 5701–5710, https://doi.org/10.1021/es034354c.

[45] M. Park, S.A. Snyder, Sample handling and data processing for fluorescent excitation-emission matrix (EEM) of dissolved organic matter (DOM), Chemosphere 193 (2018) 530–537, https://doi.org/10.1016/j.chemosphere.2017.11.069.

[46] M. Park, D. Lee, S.A. Snyder, Deconvolution of size exclusion chromatograms: new insights into the molecular weight distribution of dissolved organic matter in ozone and biological activated carbon, ACS EST Water (2020), https://doi.org/10.1021/acsestwater.0c00020.

[47] L. Bu, K. Wang, Q.-L. Zhao, L.-L. Wei, J. Zhang, J.-C. Yang, Characterization of dissolved organic matter during landfill leachate treatment by sequencing batch reactor, aeration corrosive cell-Fenton, and granular activated carbon in series, J. Hazard. Mater. 179 (2010) 1096–1105, https://doi.org/10.1016/j.jhazmat.2010.03.118.

[48] F.J. Rodríguez-Vidal, M. García-Valverde, B. Ortega-Azabache, Á. González-Martínez, A. Bellido-Fernández, Characterization of urban and industrial wastewaters using excitation-emission matrix (EEM) fluorescence: searching for specific fingerprints, J. Environ. Manag. 263 (2020), 110396, https://doi.org/10.1016/j.jenvman.2020.110396.

[49] Z. Chen, D. Li, Q. Wen, Investigation of hydrolysis acidification process during anaerobic treatment of coal gasification wastewater (CGW): evolution of dissolved organic matter and biotoxicity, Sci. Total Environ. 723 (2020), 137995, https://doi.org/10.1016/j.scitotenv.2020.137995.

[50] D.M. Reynolds, The differentiation of biodegradable and non-biodegradable dissolved organic matter in wastewaters using fluorescence spectroscopy, J. Chem. Technol. Biotechnol. 77 (2002) 965–972, https://doi.org/10.1002/jctb.664.

[51] S.A. Huber, A. Balz, M. Abert, W. Pronk, Characterisation of aquatic humic and non-humic matter with size-exclusion chromatography–organic carbon detection–organic nitrogen detection (LC-OCD-OND), Water Res. 45 (2011) 879–885, https://doi.org/10.1016/j.watres.2010.09.023.

[52] S.R. Freeman, F. Jones, M.I. Ogden, A. Oliviera, W.R. Richmond, Effect of benzoic acids on barite and calcite precipitation, Cryst. Growth Des. 6 (2006) 2579–2587, https://doi.org/10.1021/cg060186z.

[53] B. Aftab, J. Hur, Unraveling complex removal behavior of landfill leachate upon the treatments of Fenton oxidation and MIEX® via two-dimensional correlation size exclusion chromatography (2D-CoSEC), J. Hazard. Mater. 362 (2019) 36–44, https://doi.org/10.1016/j.jhazmat.2018.09.017.

[54] R.M. Cory, D.M. McKnight, Fluorescence spectroscopy reveals ubiquitous presence of oxidized and reduced quinones in dissolved organic matter, Environ. Sci. Technol. 39 (2005) 8142–8149, https://doi.org/10.1021/es0506962.